



Study of Airflow in Attic Space

Submitted to:

Homeowner Protection Office

Branch of BC Housing

1701-4555 Kingsway

Burnaby, British Columbia, Canada, V5H 4V8

January 2016

Prepared by:

Fitsum Tariku, Ph.D., Principal Investigator

Emishaw D. Iffa, Ph.D., Researcher

Building Science Centre of Excellence

British Columbia Institute of Technology

3700 Willingdon Avenue

Burnaby, British Columbia, V5G 3H2

Acknowledgements

The authors are grateful for the financial support provided by HPO, branch of BC Housing, and the in-kind contribution made by the School of Construction and the Environment of the British Columbia Institute of Technology.

Executive Summary

Energy efficiency and hygrothermal performance are few of the main considerations that need to be taken into account during design and construction of an attic roof system. In the past eight to nine decades several studies have been conducted on building durable and energy efficient attic roofs. Most of these findings recommend ventilating an attic space as an ideal solution to avoid mold growth and reduce the heating/cooling load of the system, while others cite it as a potential source of problem. Recent studies on attic roof systems in marine climate of British Columbia, which are funded by the HPO, shows some relationship between attic ventilation and mould growth on roof sheathing and structure. To propose a design solution to such problem, it is important to develop advanced understanding of attic ventilation. Through the use of Computational Fluid Dynamics (CFD), this research aims to establish relationships between attic ventilation rates and temperature and airflow distribution patterns in an attic space with local climatic conditions.

In the study, the airflow distributions, the attic air and roof sheathing temperatures, the attic ventilation rates, and the heating and cooling loads of an attic roof with four attic ventilation scenarios (sealed attic, buoyancy driven attic ventilation and two buoyancy and wind driven attic ventilation cases) are examined under winter and summer weather conditions. The results of this research project lay the foundation for the on-going HPO and BCIT funded research project on energy and moisture performance analysis of attic roof systems in the interior and coastal climates of British Columbia.

The research results show that attic ventilations in both cold and coastal climates are significantly affected by wind pressure and solar gain. In the absence of wind and solar gain, buoyancy induced ventilation in the winter is more than two times of that of the summer (~4 ACH vs 1.5 ACH). In the absence of wind, attic ventilation increases as solar radiation increases. The increments due to solar radiation can be as high as 4 ACH during the summer and 2 ACH during the winter. For wind pressure of 0.6 Pa and 2 Pa, the attic ventilation rates in the winter increases by 2.5 and 5.0 times of the case with no wind pressure (only stack effect ~4 ACH). Unlike the buoyancy induced ventilation case, the wind induced ventilation is less sensitive to solar gain and delivers similar ACH in both winter and summer days. In general, baffle size (size of air gap between roof

sheathing and insulation) has an impact on attic ventilation rate and airflow distribution, but has a lesser effect on attic air temperature. The effect of baffle size is not significant when the ventilation is driven by stack-effect. For wind pressure of 2 Pa, the ACH in the attics with 2” and 3” baffle size are 38.5% and 52.5% higher, respectively, than that of an attic with 1” baffle size. From an energy perspective, the CFD simulation results show that attic ventilation in winter poses an energy penalty, whereas it benefits during the summer period by removing the hot air from the attic space and reducing cooling load and energy demand.

The CFD simulation results also shows that in addition to attic ventilation rate, wind pressure and solar radiation shape the airflow pattern in an attic space. At relatively high wind pressure (2 Pa in this report) and absence of solar gain, the incoming air enters through soffit vent and flow underneath of the roof sheathing and exit at the ridge vent without mixing with the attic air (without diluting the attic air). At lower pressure and buoyancy-driven cases, the air flows predominately over the insulation as opposed to under the roof sheathing.

Understanding of airflow pattern and local temperature distributions in the attic space and roof structure is an essential step for solving moisture problems. Building upon the knowledge acquired in this project and applying advanced modeling techniques that combine CFD and hygrothermal modeling, it is possible to identify and develop design solutions to roof sections that are susceptible to high moisture accumulation, mold damage, ice-dam effects and overheating of roof shingles that may reduce their service life.

Table of Contents

Acknowledgements.....	2
Executive Summary	3
1 Introduction.....	8
2 Mathematical Model	10
2.1 Governing Equations.....	10
3 CFD Model Benchmarking.....	12
4 Physical Model.....	16
5 CFD Simulation Setup	18
5.1 Mesh Sensitivity Check.....	18
5.2 Boundary Conditions.....	19
6 Results and Discussion	23
6.1 Temperature and Airflow Distributions in Attic Space	24
6.2 Attic Air and Roof Surface Temperature	28
6.3 Attic Ventilation Rates.....	29
6.3.1 Effect of Insulation Thickness on Attic Ventilation	31
6.3.2 Effects of Baffle Size in Attic Ventilation.....	31
6.4 Heat Flow through Attic Floor.....	34
7 Conclusion	36
8 References.....	37
9 Appendix A: Simulation results for mild climate conditions	39

List of Figures

Figure 1 Schematic diagram of heat exchange and airflow in a simplified attic system.....	10
Figure 2 Flank and Witt’s experimental setup.....	13
Figure 3. Comparison of the predicted and experimentally measured velocity profile.....	14
Figure 4. Comparison of CFD predictions and experimentally measured temperature values. ...	15
Figure 5. Physical model of attic roof considered in the study.....	17
Figure 6. Hourly temperature and solar gain profiles in a typical winter (a) and summer (b) day in cold winter and hot summer location (Ottawa), respectively	21
Figure 7. Hourly temperature and solar gain profiles in a typical winter (a) and summer (b) day in mild climate (Vancouver), respectively	22
Figure 8 Temperature and airflow fields for different attic ventilation scenarios: (a) sealed attic, (b) stack-effect, (c) 0.6 Pa wind pressure and (d) 2Pa wind pressure—a case for winter day at 12am (Ottawa).....	26
Figure 9 Temperature and airflow fields for different attic ventilation scenarios: (a) sealed attic, (b) stack-effect, (c) 0.6 Pa wind pressure and (d) 2Pa wind pressure—a case for winter day at 2:00 pm with solar gain (Ottawa).....	27
Figure 10 Average attic air temperature for different attic ventilation scenarios during a typical winter and summer day (Ottawa). Color code: green (sealed), blue (stack effect), red (0.6Pa wind pressure), black (2Pa wind pressure).....	28
Figure 11 Maximum roof sheathing for different attic ventilation scenarios during a typical winter and summer day (Ottawa). Color code: green (sealed), blue (stack effect), red (0.6Pa wind pressure), black (2Pa wind pressure)	29
Figure 12 Attic ventilation rates for different attic ventilation scenarios during a typical winter and summer day (Ottawa). Color code: blue (stack effect), red (0.6Pa wind pressure), black (2Pa wind pressure).....	30
Figure 13 Effect of solar radiation in attic ventilation rate (for cases with stack effect).....	30
Figure 14 Attic ventilation rates with different insulation thickness.....	31
Figure 15 Attic ventilation (ACH) vs attic baffle size.....	32
Figure 16 (a) - (c) air distribution in wind driven attic ventilation with an attic of baffle size 1 in, 2 in and 3 in respectively	33

Figure 17 Heat flux along the attic floor at 12:00 am (winter day--Ottawa). Color code: green (sealed), blue (stack effect), red (0.6Pa wind pressure), black (2Pa wind pressure) .. 34

Figure 18 Hourly heat flux through attic floor for different attic ventilation scenarios during a typical winter and summer day (Ottawa). Color code: green (sealed), blue (stack effect), red (0.6Pa wind pressure), black (2Pa wind pressure)..... 35

Figure 19 Average attic air temperature for different attic ventilation scenarios during a typical winter and summer day—Mild climate (Vancouver). Color code: green (sealed), blue (stack effect), red (0.6Pa wind pressure), black (2Pa wind pressure)..... 39

Figure 20. Maximum roof sheathing temperature for different attic ventilation scenarios during a typical winter and summer day—Mild climate (Vancouver). Color code: green (sealed), blue (stack effect), red (0.6Pa wind pressure), black (2Pa wind pressure) .. 40

Figure 21 Attic ventilation rates for different attic ventilation scenarios during a typical winter and summer day—Mild climate (Vancouver). Color code: blue (stack effect), red (0.6Pa wind pressure), black (2Pa wind pressure) 40

Figure 22 Effect of solar radiation in attic ventilation rate (for cases with stack effect)—Mild climate..... 41

Figure 23 Hourly heat flux through attic floor for different attic ventilation scenarios during a typical winter and summer day—Mild climate (Vancouver). Color code: green (sealed), blue (stack effect), red (0.6Pa wind pressure), black (2Pa wind pressure) .. 41

List of Tables

Table 1. The $k-\omega$ turbulent model coefficients used in in the model..... 12

Table 2. Thermal conductivity and heat capacity of the attic roof layers..... 17

Table 3. Percentage error and percentage time saved by different mesh sizes..... 19

Table 4. Grashof’s numbers of the four simulation cases at different conditions 24

1 Introduction

It is a common practice to design and build sloped roofs with openings at the soffits and the ridges to promote airflow through the attic roof system. In cold and mild climates, the airflow is intended to control moisture in the attic space whereas in the warm climate to cool the roof and increase its thermal performance. Ventilating attics can also minimize the ice dams formed near eaves and prolong roof shingles service life. Ventilating for one of these drivers can have a contrary effect on the other objectives. For example ventilating the attic to remove the condensation moisture during winter can increase the heating load. These two different purposes of ventilation can be achieved using regulated or adaptive ventilation systems. But most residential buildings with natural ventilation keep their vent configuration and ratios constant throughout the year.

Teesdale [1] is believed by many to be the first researcher to recommend ventilation and the usage of suitable vapor barriers. Rogers [2] in 1938 assessed the common understanding that has spread during the time ‘insulation draws water into the walls and roofs’. He recommended possible ways of preventing condensation while the attic space is ventilated. Roodvoets [3] attempted to develop a protocol to determine the driving forces to add additional ventilation during retrofitting in mixed climates. He suggested that five meters per second wind speed is considered as sufficient ventilation to remove all the unwanted moisture accumulated in the residential occupied space. Forest and Walker [4] measured the ACH (air exchange per hour) value for attic with intentional venting area and sealed attic at the research houses at the University of Alberta. Their findings showed the ventilation rates are also within the range of 0 to 7 ACH for a house that had no intentional venting area added to the roof assembly. A ventilation rate of 0 to 50 ACH was measured for the attic with a venting area of 1:300 ratio to attic floor. Measurement results by Roppel et. al. for ventilation rate using a tracer gases lie in a range of 1 to 5 ACH [5]. Lstiburek recommended the air change in a perfectly built and vented attic (code 1:300 ratio) should result in an average air change rate of 3 to 6 ACH [6].

Based on Peavy’s [7] thermal performance predicting model and Wilkes’ reports [8,9], researchers from Oakridge National Lab developed standard practice to estimate heat loss or gain through attic floors with a computer model called AtticSim [10]. A mathematical attic ventilation model called ATTIX was developed by Forest and Walker [4] based on mass balance of air entering and leaving

the attic space. These attic models consider the attic as mixed air space with uniform temperature and humidity distribution.

Recently, several researchers such as Wang et al. [11, 12] and Galagliano et al. [13] used Computational Fluid Dynamics (CFD) to study various attic vent configurations in a simplified attic model, which assume a shape of isosceles triangle with the two inclining sides representing the roof while the horizontal side symbolizes the ceiling. Although this is a development in the right direction, the approach excludes the flow dynamics at the entry and exit of the attic space. The actual airflow pattern depends on the pressure and temperature conditions across the entire domain (entry to exit points). In this research, buoyancy driven and wind-induced attic ventilations in typical winter and summer day of cold and mild climate regions, which are represented by Ottawa and Vancouver, respectively, are investigated. The airflow and temperature distributions in the attic in response to hourly varying thermal boundary conditions (temperature and solar radiation) are discussed. The analysis is carried out using a two-dimensional (2D) attic roof geometry that includes the soffit and the baffle regions as part of the computational domain.

In the next sections, first, the COMSOL Multiphysics 4.4¹ CFD mathematical models, which is used in this report, are presented along with a benchmark exercise, and then the physical description of an attic roof considered in the study and the procedures that are followed for an optimum computational model are discussed, and finally the CFD model is used to quantify the air-exchange-per-hour as well as to provide the temperature and airflow distributions in attic spaces during typical winter and summer days.

¹<http://www.comsol.com/>

2 Mathematical Model

In Figure 1 the typical thermal loads on an attic system along with openings for air exchange are shown. Due to the different thermal loads on the roof, ceiling and incoming air, the airflow in the attic is non-isothermal. Thus, the energy and momentum balance equations for the air in the attic need to be solved along with the conduction heat transfers through the attic floor layers and roof structures. Such heat transfer and fluid flow problem is defined as a conjugate heat transfer. In the following sections the governing equations that are used to solve the temperature and airflow field in the attic space and accompanying structures are presented.

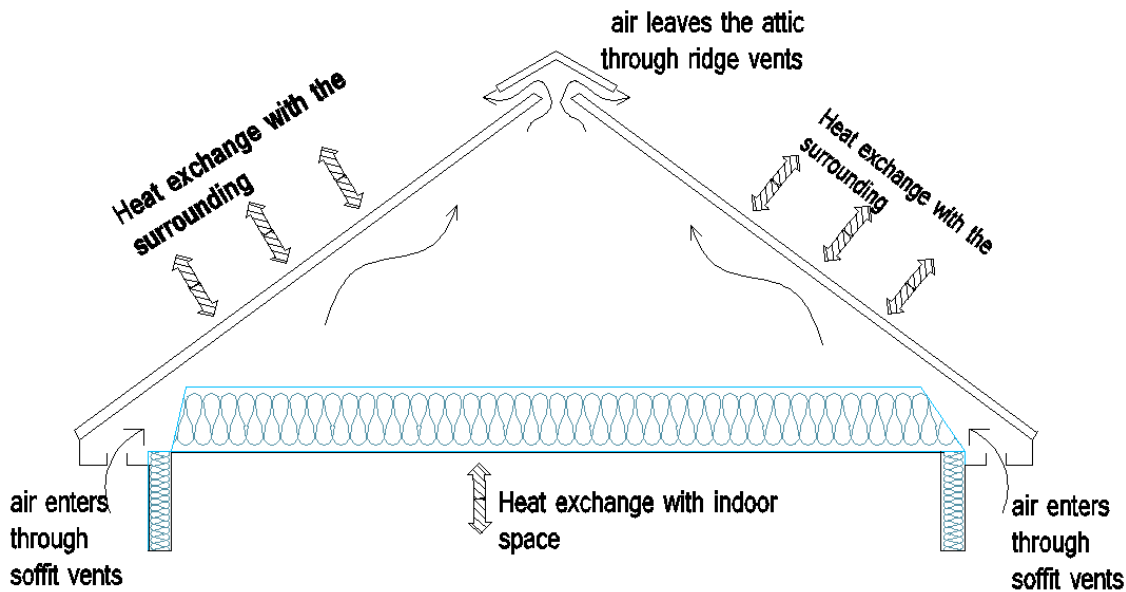


Figure 1 Schematic diagram of heat exchange and airflow in a simplified attic system

2.1 Governing Equations

The fluid flow in the attic can be characterized as incompressible flow. The governing equations for the mass, momentum and energy conservation in a two-dimensional flow are given in Equation 1, Equation 2 and Equation 3, respectively. These momentum equations, which can also be referred as Reynolds-Average Navier-Stokes (RANS) equations, are derived from the general Navier-Stokes equations after applying Reynolds averaging technique. Thus, in the equations, the

u , v , and T are mean values of velocity and temperature and μ is the dynamic viscosity of air. The Reynolds stresses are modeled analogues to shear stresses using eddy viscosity (μ_T). The flow in the attic can be mixed flow, where both forced and buoyancy driven flows can coexist. To capture the buoyancy driven flow, the Boussinesq approximation is applied into the RANS momentum equation in the y-direction, which effectively assumes constant density (ρ^o) in all terms except the body force and thereby introduces a buoyancy term, $g(\rho - \rho^o)$, in the momentum balance equation g is the gravitational acceleration and ρ is temperature dependent density, which is calculated based on ideal gas law.

$$\frac{\partial u}{\partial x} + \frac{\partial v}{\partial y} = 0 \quad (1)$$

$$\rho^o \left(\frac{\partial u}{\partial t} + u \frac{\partial u}{\partial x} + v \frac{\partial u}{\partial y} \right) = - \frac{\partial p}{\partial x} + (\mu + \mu_T) \left(\frac{\partial^2 u}{\partial x^2} + \frac{\partial^2 u}{\partial y^2} \right) \quad (2)$$

$$\rho^o \left(\frac{\partial v}{\partial t} + u \frac{\partial v}{\partial x} + v \frac{\partial v}{\partial y} \right) = - \frac{\partial p}{\partial y} + (\mu + \mu_T) \left(\frac{\partial^2 v}{\partial x^2} + \frac{\partial^2 v}{\partial y^2} \right) + g(\rho - \rho^o)$$

$$\rho^o C_p \left(\frac{\partial T}{\partial t} + u \frac{\partial T}{\partial x} + v \frac{\partial T}{\partial y} \right) = (\lambda + \lambda_T) \left(\frac{\partial^2 T}{\partial x^2} + \frac{\partial^2 T}{\partial y^2} \right) \quad (3)$$

The turbulent model used in this report is the k - ω two equation eddy viscosity turbulent model. This model is found to be robust for isothermal and non-isothermal flows in enclosed space [17]. In this model the eddy viscosity is defined as $\mu_T = \rho \frac{k}{\omega}$, where k is the turbulent kinetic energy and ω is the dissipation per unit turbulent kinetic energy. The eddy conductivity, λ_T , in the energy balance equation is defined by the turbulent Prandtl number and eddy viscosity values $Pr_T = C_p \frac{\mu_T}{\lambda_T}$. The governing equations for k and ω as well as the Kays-Crawford equation for turbulent Prandtl number that are implemented in the COMSOL Multiphysics and used in this work are given in Equation 4, 5 and 6, respectively, and the accompanying coefficients are shown in Table 1. C_p is the specific heat of air. The heat transfer through solid components of the attic structure is computed by setting, u , v and λ_T values to zero in the energy balance equation, Equation 3.

$$\rho^o \left(\frac{\partial k}{\partial t} + u \frac{\partial k}{\partial x} + v \frac{\partial k}{\partial y} \right) = (\mu + \mu_T \sigma_k^*) \left(\frac{\partial^2 k}{\partial x^2} + \frac{\partial^2 k}{\partial y^2} \right) + P_k - \rho^o \beta_0^* k \omega \quad (4)$$

$$\rho^o \left(\frac{\partial \omega}{\partial t} + u \frac{\partial \omega}{\partial x} + v \frac{\partial \omega}{\partial y} \right) = (\mu + \mu_T \sigma_\omega^*) \left(\frac{\partial^2 \omega}{\partial x^2} + \frac{\partial^2 \omega}{\partial y^2} \right) + \alpha \frac{\omega}{k} P_k - \rho \beta_o \omega^2 \quad (5)$$

$$\text{where } P_k = \mu_T [\nabla u : (\nabla u + (\nabla u)^T)]$$

$$Pr_{T\infty} = \left(\frac{1}{2Pr_{T\infty}} + \frac{0.3}{\sqrt{Pr_{T\infty}}} \frac{c_p \mu_T}{\lambda} - \left(0.3 \frac{c_p \mu_T}{\lambda} \right)^2 (1 - e^{-\lambda/(0.3c_p \mu_T \sqrt{Pr_{T\infty}})})^{-1} \right)^{-1} \quad (6)$$

where Prandtl number at infinity is $Pr_{T\infty} = 0.85$ and λ is conductivity

Table 1. The k - ω turbulent model coefficients used in in the model

Coefficient	Value	Coefficient	Value
α	0.52	β_o^*	0.09
σ_k^*	0.5	k_ν	0.41
σ_w	0.5	B	5.2
β_o	0.072		

The conjugate heat transfer model is used to describe heat transfer in solids and non-isothermal flow in the fluid. The heat transfer module is tightly coupled with the turbulent fluid flow model and described in Equation 3. In addition to conduction and convection, the surface-to-surface radiation exchange between the inner surface of the roof sheathing and the top surface of the ceiling insulation are considered in this report.

3 CFD Model Benchmarking

Most unvented attic experimental and numerical simulation models assume a shape of isosceles triangle with the two inclining sides representing the roof while the horizontal side symbolizes the ceiling. Flack et al. [18] conducted experimental measurement of turbulent natural convection in

attic like shape with temperature variation from below. The buoyancy flow inside the triangular shape was visualized using Schlieren and laser velocimetry tools.

In this report, the velocity and temperature profiles in the triangular enclosure reported by Flack [18, 19] are used for benchmarking of the CFD model presented in the previous section. This triangular enclosure can seamlessly represent the sealed attic model used in this report.

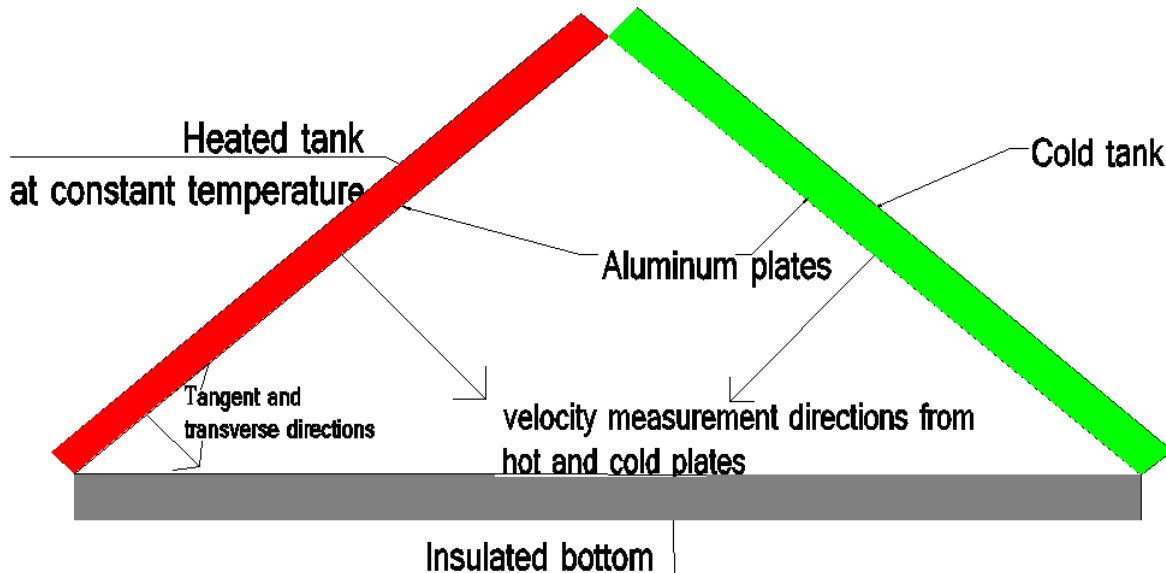


Figure 2 Flack and Witt's experimental setup

In his experiment, Flack used air filled triangular enclosure built from two constant temperature tanks and one horizontal insulated bottom as shown in Figure 2. Wollaston prism Schlieren interferometer was used to measure the heat transfer rates in the same enclosure. Polished aluminum plates were used to form the two inclined sides of the triangular enclosure. Two dimensional velocity profiles, in tangent and transverse directions of the inclined plane, were measured using Laser Velocimeter. The inclined surfaces are subjected to hot temperature on one side and cold temperature on the other side. In Figure 3, the Laser Velocimeter measurements of velocity profiles in perpendicular direction from the hot and cold plates at midpoints of the isothermal inclined surfaces are presented along with the CFD simulation results of the corresponding locations. In this experiment [18], the hot and cold temperatures of the inclined plate are set at a constant temperature of 64°C and 0°C respectively. η and U are normalized

space and velocity values that are defined as a function of directions normal and tangential to isothermal surface, length of the isothermal surface, Grashof's number and average velocity.

$$\eta = \frac{Y}{(4X)^{\frac{1}{4}}} \quad \text{where } Y = \frac{Gr^{1/4}y}{L} \text{ and } X = \frac{x}{L} \quad (7)$$

$$U = \left(\frac{Gr}{4X}\right)^2 \bar{u}$$

x and y are tangent and normal directions to an isothermal surface

Gr Grashof's number

L is length of the isothermal surface

\bar{u} is normalized velocity

As can be seen in the figure, the model predictions are in good agreement with the experimental measurements. The maximum root mean square (RMS) error between the measurement and simulation results is only 2.1%.

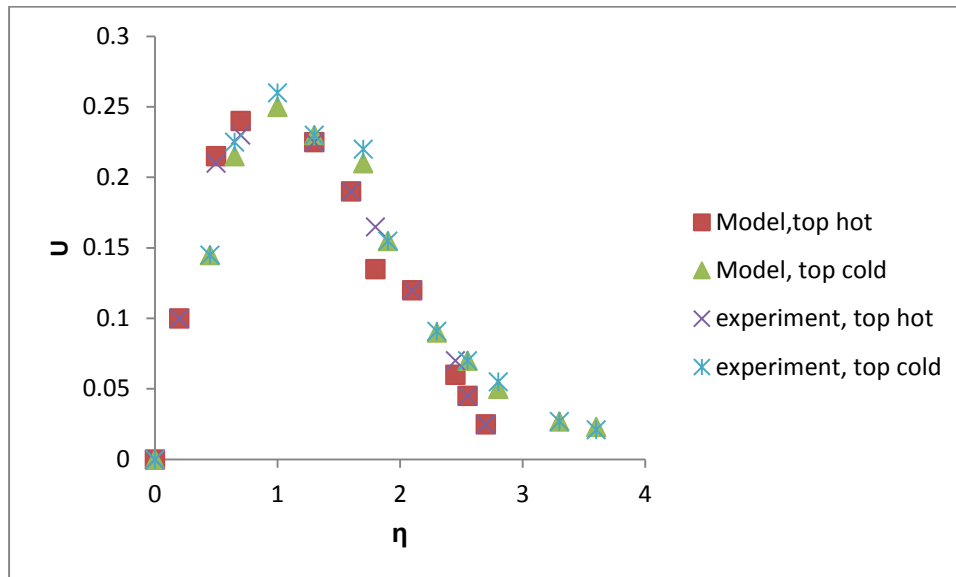


Figure 3. Comparison of the predicted and experimentally measured velocity profile.

As an additional model validation exercises, two experimental cases with boundary conditions that give different velocity and temperature distributions are considered. The experiments are done by Flanks [19] using the experimental setup discussed above. In one of the experiment, the horizontal plate is kept at 20°C and the inclined plates are kept at 40°C, which is referred here as ‘top hot’, and in the second one the inclined plates are maintained at 0°C and the horizontal plate at 20°C, which is referred here as ‘top cold’ case. The experimentally measured temperature distributions along the centerline of the triangular enclosure in the two experiments are normalized and shown in Figure 4. For comparison purpose, the normalized CFD simulation results are superimposed on the same figure. As can be seen in the figure, the CFD simulation results agree very well with the measured data.

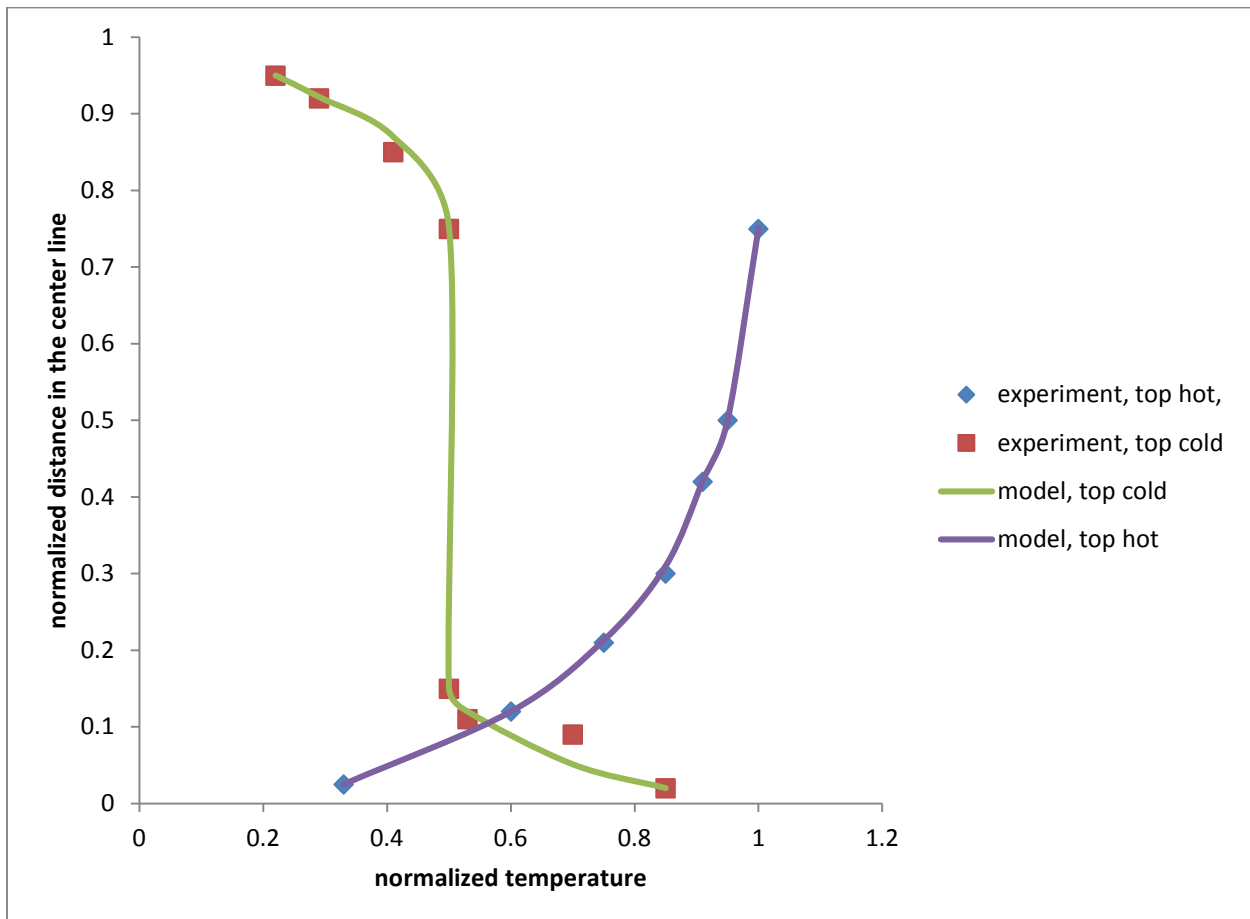


Figure 4. Comparison of CFD predictions and experimentally measured temperature values.

4 Physical Model

In this report, a sloped roof with 4:12 pitch and an attic floor area of 74.32 m^2 (800 ft^2) is considered for the study, Figure 5. According to the Canadian National Building Code [20] (NBC 2010), roofs with insulation between the interior ceiling and roof sheathing require ventilation. For the roof system considered here, the design attic ventilation opening area is required to be $1/300$ of the attic floor area. Accordingly, the roof with attic floor area of 74.32 m^2 (800 ft^2) will need to have 0.25 m^2 (2.7 ft^2) area of opening for ventilation to satisfy the Code requirement. The code also requires that the roof shall have equal vent opening areas on the opposite side of the roof space; and also requires that the ventilation openings at the top and bottom of the roof space each to be over 25% of the total ventilation area. The common design practice is to allocate 60% of the ventilation opening at the bottom (soffit) and 40% at the top (ridge) of the roof space. In this report, following the current practice, the soffit and ridge vent opening areas are assumed to be 0.15 m^2 (0.075 m^2 per side) and 0.09 m^2 , respectively, which are equivalent to having 10 mm and 15 mm continuous openings at the soffit and ridge level as presented in Figure 5. To prevent the insulation from blocking airflow at the bottom of the roof, a baffle with 51 mm depth and 91 mm length is placed between the sheathing and the insulation. This attic system considered in the study work focuses on existing houses. In this work, the attic is assumed to be of an existing house and insulated according to the 1997 MNECC (Model National Energy Code of Canada): 211 mm depth of loose cellulose insulation of RSI 5.3 (R-30) at the center and 97 mm at the eave edge. The attic floor is drywall, and the roof cover is built with shingles and plywood sheathing. A complete roof system includes vapor barrier and sheathing membrane, which are not shown here as their effect on heat transfer through the roof assembly is negligible. The thermal conductivity and heat capacity of the drywall, insulation and plywood sheathing are given in Table 2. The solar absorptivity and emissivity properties of the roof shingles are 0.8 and 0.9, respectively.

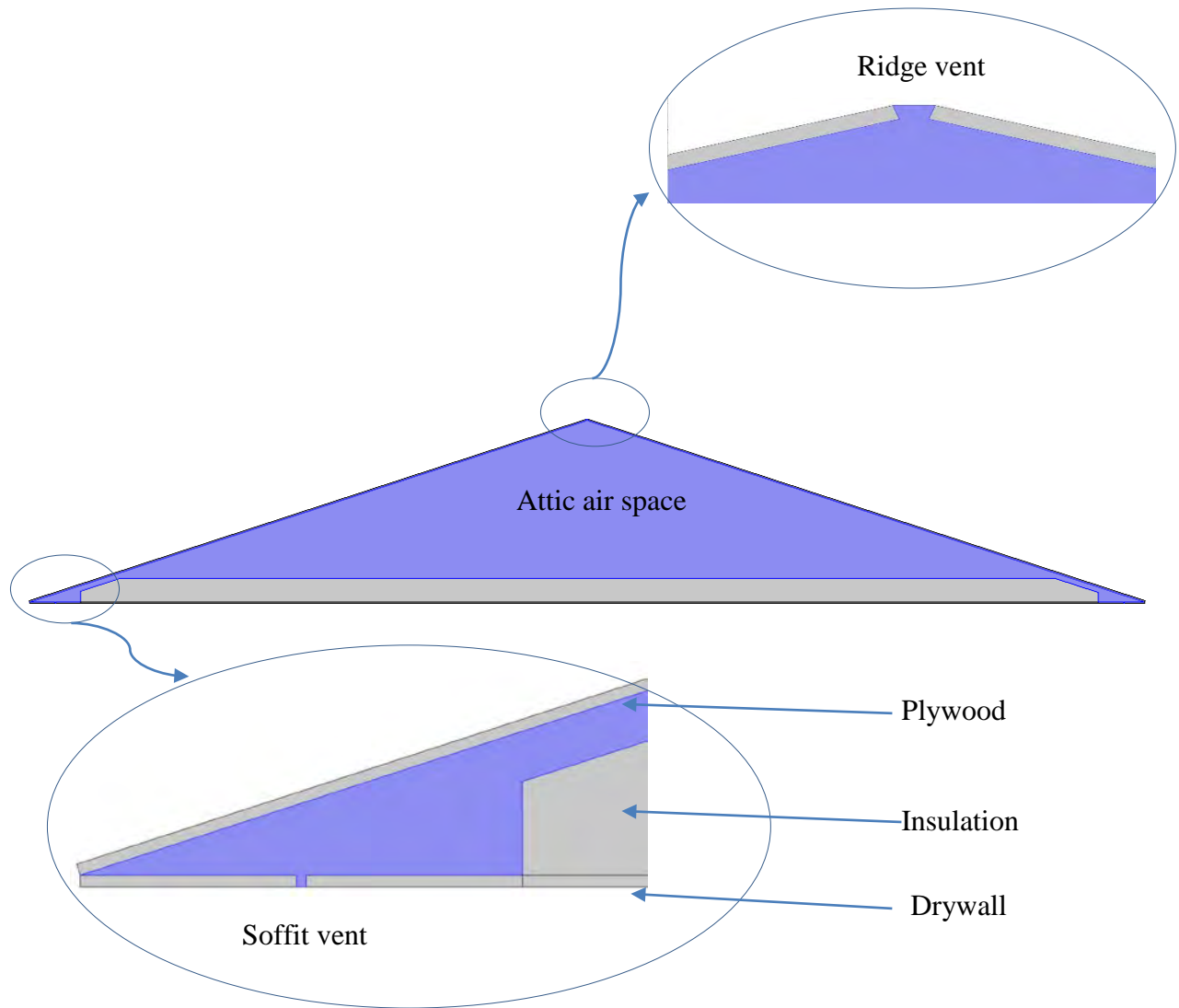


Figure 5. Physical model of attic roof considered in the study.

Table 2. Thermal conductivity and heat capacity of the attic roof layers

	Thickness (m)	Thermal conductivity (W/(m.K))	Heat capacity (J/(kg.K))
Drywall	0.0125	0.177	1097
Loose Cellulose Insulation	0.211	0.04	1007
Plywood	0.0125	0.13	1507

5 CFD Simulation Setup

The physical attic roof model shown in Figure 5 is drawn in the COMSOL GUI and form the computational domain. The computational domain is discretized with triangular finite elements mesh and solved with time-dependent solver, as the boundary conditions considered in this report are time dependent. The implicit time stepping scheme uses Backward Differentiation Formulas (BDF) method to update the solutions in time.

5.1 Mesh Sensitivity Check

A user controlled mesh is created and sizes and types of grids are developed for different regions of the computational domain to allow COMSOL to solve the model accurately and economically. The attic space has a finer mesh size as compared with the solid parts of the attic such as drywall, roof sheathing and insulation. This approach increased the modeling accuracy because the fluid dynamics model demands finer mesh size. Regions around the inlet and the outlet vents are meshed with extra fine mesh sizes as they are relatively small in size and air jet enters and leaves the system at these ports at relatively high velocity. In addition, boundary layer meshes are envisaged near the solid boundaries and corner refinement meshes are included at corners of the fluid flow boundary.

To make sure an optimal mesh size, beyond which the solution accuracy does not improve significantly and becomes mesh size independent, is used in the modeling, a mesh size sensitivity test is conducted by comparing the results of three models with different number of elements. The mesh sizes used for comparison were 21,256 elements, 43,675 elements and 76,312 elements. The first two models mass flow rate, average attic temperature value and processing time are compared with the most dense mesh model. In comparison to the model with ~76,000 element, the model with 43,675 elements has small mass flow rate and average attic temperature differences (1.89% and 1.34%, respectively) when compared with the model with 21,256 elements. This can be considered as very small difference for a model with almost as half of the number of mesh elements. The computational time saved by using 21,256 elements compared to 43,675 elements is marginal. This outcome prompts to use an attic model consisting of 43,675 elements throughout this study. These findings are tabulated in Table 3.

Table 3. Percentage error and percentage time saved by different mesh sizes

Mesh size	% difference compared to most dense mesh size (76,312 elements)		% time saved compared most dense mesh size (76,312 elements)
	Mass flow rate	Avg. Attic temperature	
21,256 elements	2.73	2.01	16.14
43,675 elements	1.89	1.34	17.35

5.2 Boundary Conditions

The problem under this study involves an attic enclosure exposed to variable thermal loading. It also includes inlet vents that allow an air jet to enter in to the attic space by wind pressure or stack effect and outlet vents to remove air from the attic. These boundary conditions are used by the coupled fluid flow (Navier -Stokes) and heat transfer (energy balance) mathematical models. The boundary conditions are generated based on Ottawa and Vancouver weather data, which represent locations with extreme (cold winter and hot summer days) and mild temperature conditions as the interior and the coastal regions of British Columbia experiences.

To assess the temperature and airflow (ACH) conditions in the attic roof during day and night times of a typical winter and summer day, hourly temperature data are constructed using Ottawa’s January and July monthly averages and maximum temperature differences following the ASHRAE Fundamentals (2013) [21] procedure for generating design day data. The same procedure is applied for Vancouver but using August instead of July for the summer period. In Figure 6 and Figure 7 the hourly temperature along with global horizontal solar radiation data for Ottawa and Vancouver, respectively, are presented. The solar gains on the roof surface are calculated based on their orientations and inclinations.

Considering a building with its ridge runs from north to south the left and the right sides of the attic roof model represent the roof parts facing east and west, respectively. In the simulations, the east and the west roof surfaces receive different solar gains that vary hourly. The variable thermal loads on the roof are calculated as a composition of heat flux terms from convection heat transfer,

long-wave radiation exchange and solar gain values. The heat flux values at the left and right side of the roof are equated as:

$$Q_l = h_{out}(T_{out} - T) + \alpha Solgain_L \quad (7)$$

$$Q_r = h_{out}(T_{out} - T) + \alpha Solgain_R$$

The first term in the left hand side represents the combined effects of the convective and long-wave radiation heat transfers using an equivalent surface transfer coefficient, h_{out}

where

Q_l : heat flux on the left side of the roof

Q_r : heat flux on the right side of the roof

h_{out} : outside heat transfer coefficient

T_{out} : outside temperature

T : attic temperature

$Solgain_L$: solar gain on the left side of the roof

$Solgain_R$: solar gain on the right side of the roof

α : Solar absorption coefficient of the outside surface of the roof shingles

Similarly, the heat transfer between the indoor space and the ceiling is represented by Equation 8.

$$Q_c = h_{in}(T_{in} - T) \quad (8)$$

where:

Q_c : heat flux passes through ceiling

h_{in} : internal surface coefficient

T_{in} : conditioned space temperatures

In this work, the conditioned space temperature is set to 21°C, and heat transfer coefficient values of 25 W/(m².K) and 8 W/(m².K) are used for the exterior and interior surfaces, respectively.

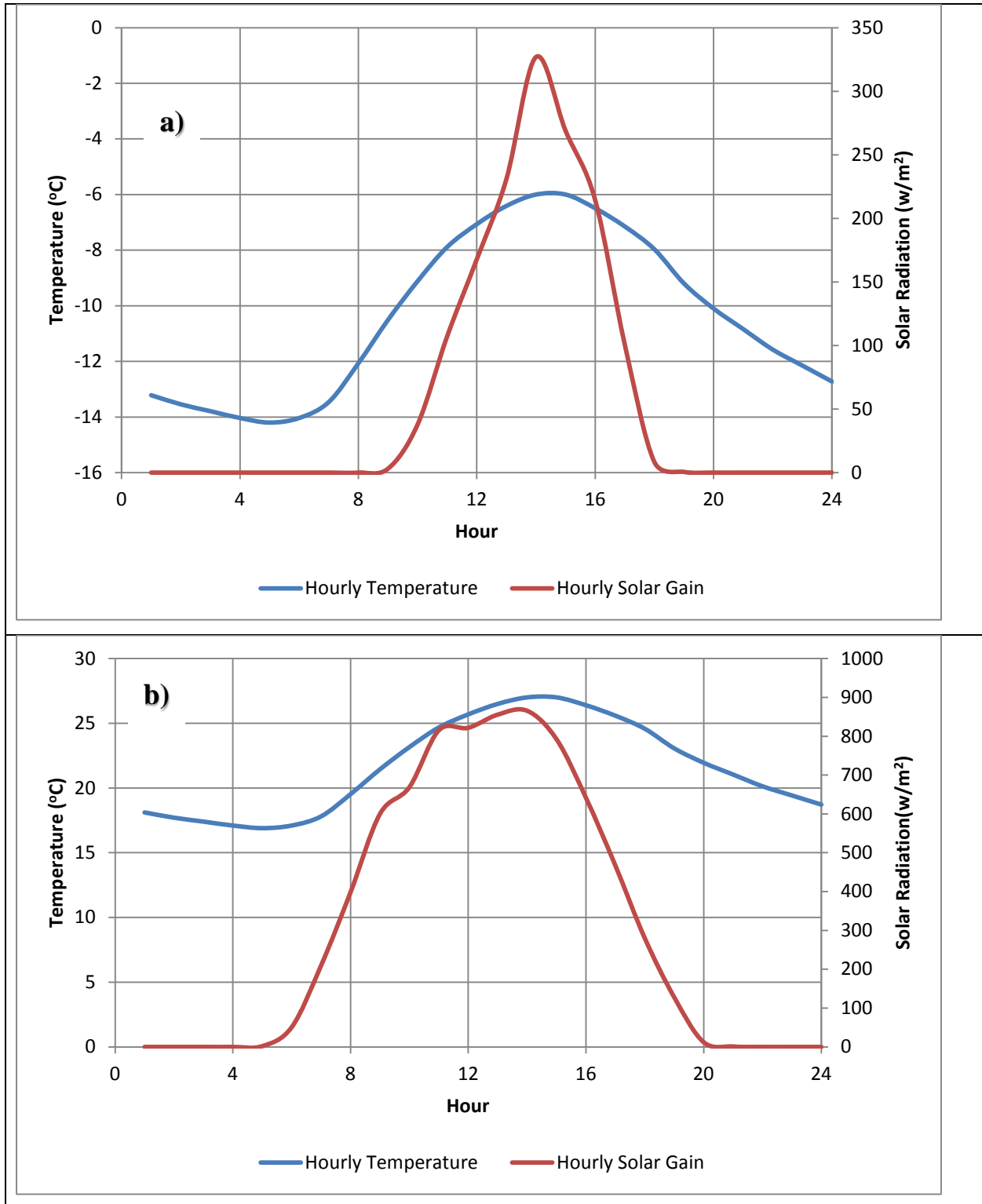


Figure 6. Hourly temperature and solar gain profiles in a typical winter (a) and summer (b) day in cold winter and hot summer location (Ottawa), respectively

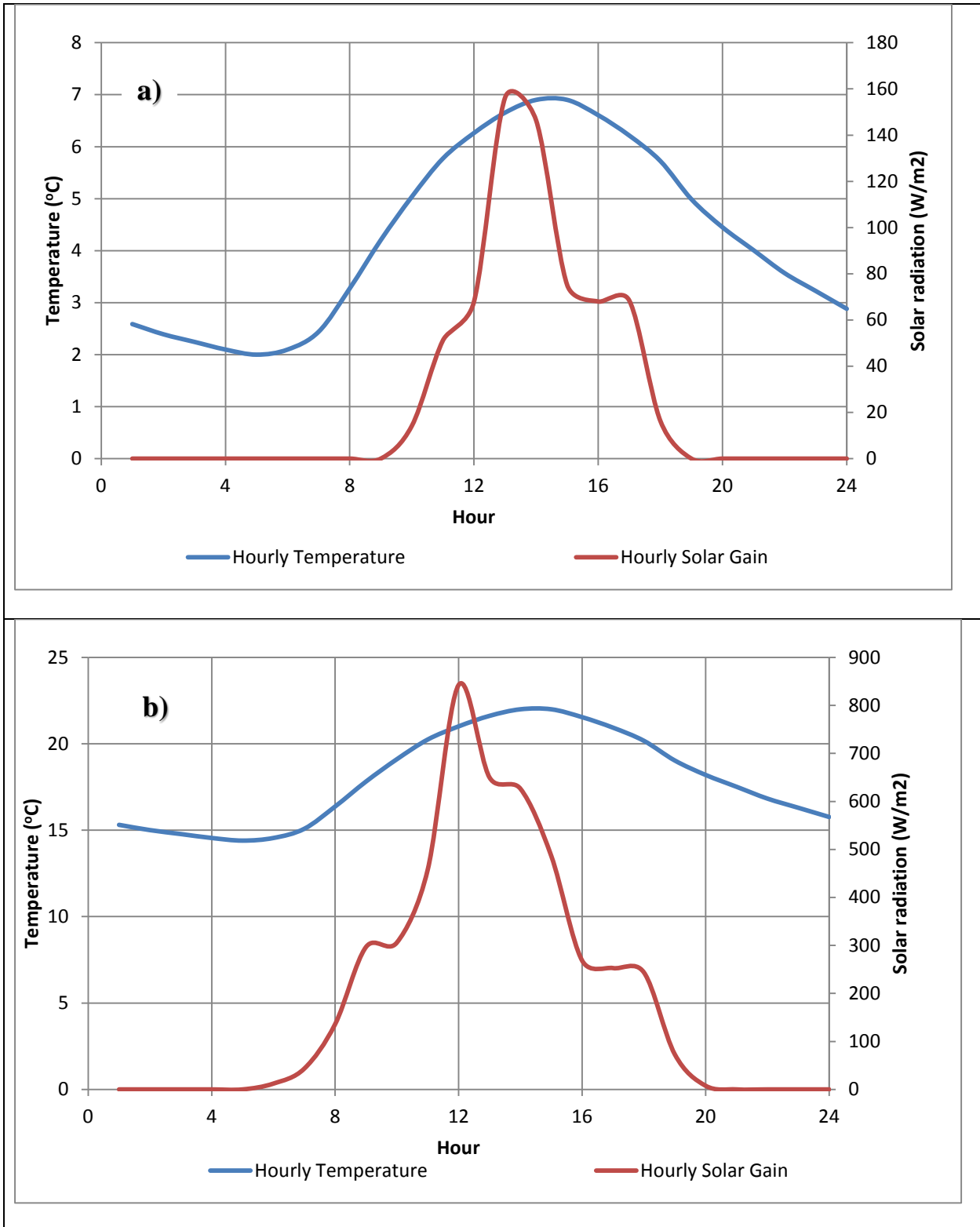


Figure 7. Hourly temperature and solar gain profiles in a typical winter (a) and summer (b) day in mild climate (Vancouver), respectively

For airflow calculation, pressure boundary conditions are applied at the soffits and ridge openings. The surface pressures are calculated from the local pressure coefficients and wind speed at roof level, Equation 9. In this work, the local pressure coefficients from ASHRAE Fundamentals (2013) [21] are used. Accordingly, pressure coefficient values of 0.8 and -0.43 are used at the wind-ward and lee-ward soffit openings, respectively, and a pressure coefficient of -1 is used at the ridge opening. In this study two wind speeds, a moderate (1.8 m/s) and a low (1 m/s) wind speed conditions, are considered based on the Building Science Centre of Excellence wind speed measurement results. The corresponding dynamic pressures $\left(\frac{\rho U_r^2}{2}\right)$ at the roof height are 2 Pa and 0.6 Pa, respectively. In simulation cases with no wind pressure, the pressure boundary conditions at all openings will be atmospheric pressure and defined as gauge pressure of 0 Pa.

$$p_s = Cp_l \frac{\rho U_r^2}{2} \quad (9)$$

Where p_s is surface pressure; Cp_l local pressure coefficient; U_r wind speed at roof height and ρ air density.

6 Results and Discussion

In this section, the simulation results of four different venting scenarios in typical winter summer day of Ottawa are discussed. Simulation results based on Vancouver weather data are presented in Appendix A. The chosen boundary conditions and the simulation results apply to the interior and coastal regions of British Columbia that have similar boundary conditions: cold winter and hot summer, and mild winter and summer, respectively.

In the first case, the attic is sealed and there are no inlet and outlet vents. In the second case, attic ventilation takes place due to buoyancy only. In the third and fourth cases wind driven ventilations are investigated at 2 Pa and 0.6 Pa. The wind is assumed to blow from east to west (left to right in Figure 5. For the last three cases, the contribution of solar driven attic ventilations during a typical winter and summer day are presented.

6.1 Temperature and Airflow Distributions in Attic Space

Natural convection flow in attic can be generated from the insulation top surface or under side of roof sheathing depending on their temperature. Although these situations in general correspond to winter and summer cases, sheathing temperature can be significantly higher than the top of insulation surface during winter period due to heating up by the solar radiation. The Grashof's numbers for the four simulation cases during the night (no solar gain) and 2:00 pm (when there is solar radiation) are presented in Table 4. The length of the rafter and the roof height are used as characteristic lengths for calculation of Grashof's number for the cases with and without solar radiation, respectively. As can be seen from the table, the Grashof numbers in all cases are greater than $2.5E+8$, and consequently the flows are near turbulent or fully turbulent.

Table 4. Grashof's numbers of the four simulation cases at different conditions

Attic ventilation scenarios	Winter		Summer	
	12:00 AM (no solar gain)	2:00 PM (with solar gain)	12:00 AM (no solar)	2:00 PM (with solar gain)
Sealed attic	2.0E+9	7.5E+11	4.6E+8	1.5E+12
Buoyancy only	2.5E+9	1.3E+12	2.5E+8	2.8E+12
Wind pressure at 0.6 Pa	1.2E+9	1.5E+12	2.5E+8	3.0E+12
Wind pressure at 2 Pa	1.2E+9	1.7E+12	3.2E+8	3.3E+12

The temperature and airflow fields in an attic with different ventilation scenarios are shown in Figure 8. The results represent a condition in a winter day with no solar radiation. Although the temperature contour plots are similar, the airflow patterns are quite different. In the attic case with 2Pa wind pressure (Figure 8, d), the incoming air seems to have enough momentum to flow along the underside of the sheathing to the ridge outlet. As the wind pressure reduced to 0.6 Pa (Figure 8, c), the incoming cold air stream loses its inertia and changes course, and flows over the insulation surface and underside of the opposite roof sheathing by buoyancy action before exiting at the ridge opening. When there is no wind pressure, buoyancy force creates a symmetrical airflow pattern in the vented attic space with relatively warm existing along the symmetry line (Figure 8,

b). In sealed attic two flow regions with different sizes are created (Figure 8, a). Figure 9 shows the temperature and airflow patterns in the attic spaces of the four attic operation scenarios at 2:00 pm of a winter day with solar gain. As can be seen in Figure 9, the airflows in all cases are primarily due to solar driven buoyancy force, which draws air to flow underside of the solar heated sheathing including the case with a wind pressure of 2Pa (Figure 9, d). Notable flow pattern differences at 12:00 am (Figure 8,) and 2:00 pm (Figure 9). The cold air stream with 2 Pa (Figure 8 (d)) wind pressure doesn't flow near the left roof sheathing as in Figure 7(d) instead forced to change flow path and exit after flowing under the heated sheathing (right side). The airflow in the sealed attic (Figure 8, d) has changed from two flow regions to one. Simulation results of the four attic operation scenarios in a summer day yielded similar airflow patterns.

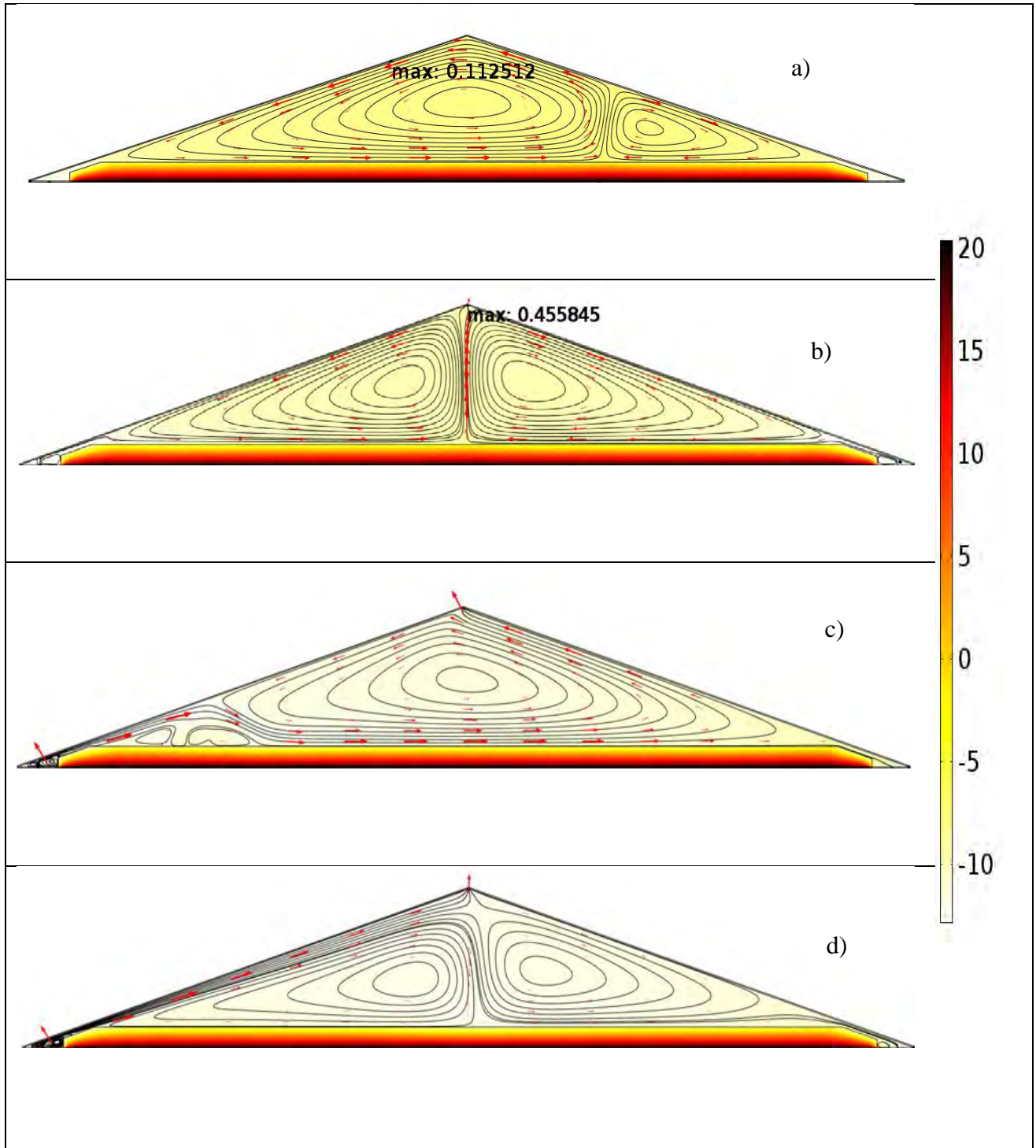


Figure 8 Temperature and airflow fields for different attic ventilation scenarios: (a) sealed attic, (b) stack-effect, (c) 0.6 Pa wind pressure and (d) 2Pa wind pressure—a case for winter day at 12am (Ottawa)

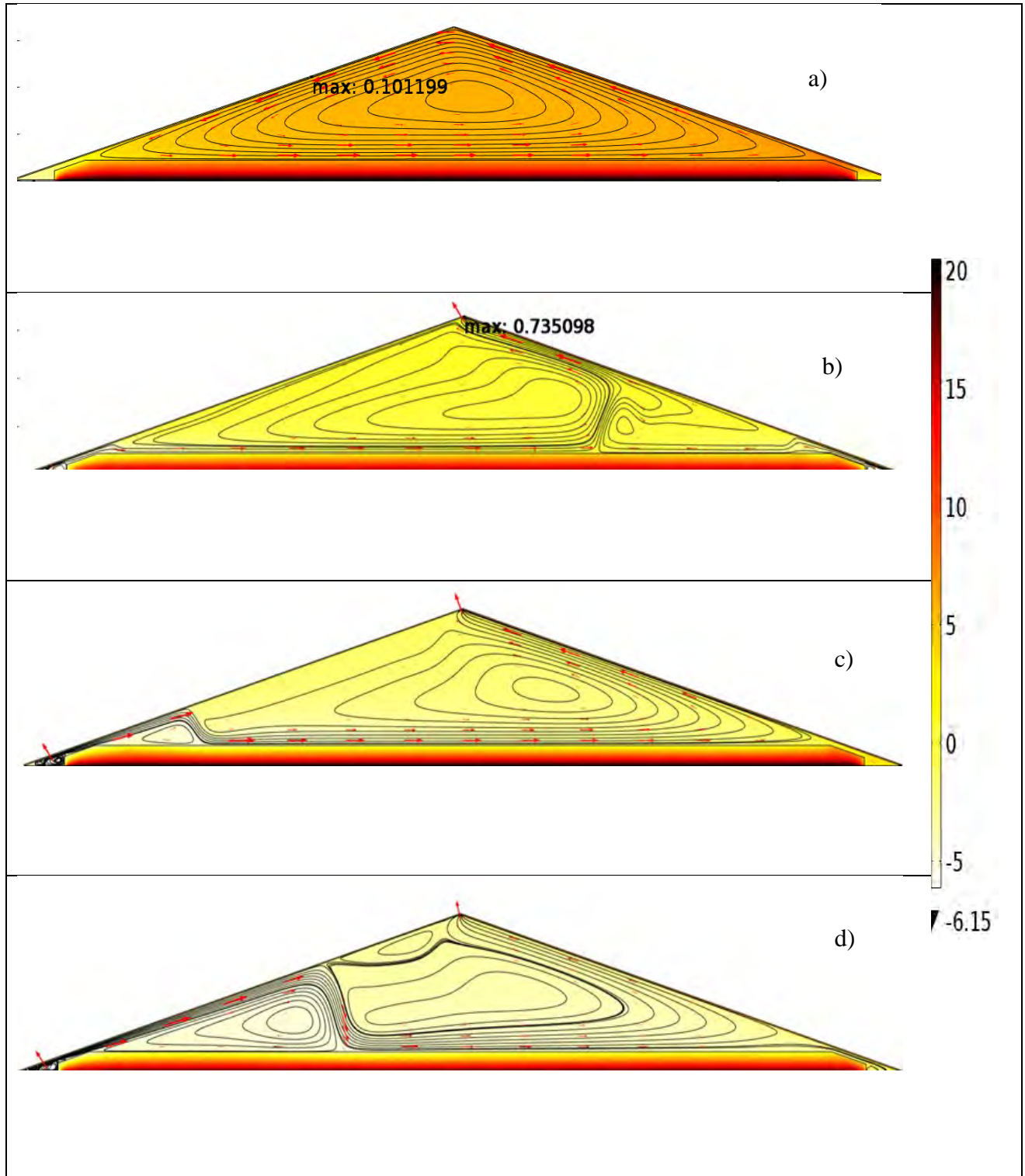


Figure 9 Temperature and airflow fields for different attic ventilation scenarios: (a) sealed attic, (b) stack-effect, (c) 0.6 Pa wind pressure and (d) 2Pa wind pressure—a case for winter day at 2:00 pm with solar gain (Ottawa).

6.2 Attic Air and Roof Surface Temperature

The average attic air temperatures during a winter and a summer day for the four attic operation scenarios are shown in Figure 10. As can be seen in the figures, during both winter and summer, the attic air temperature is the highest in the sealed attic and the lowest in the wind ventilated cases. The temperature differences increase with solar radiation gain, and reaches to maximum of 10°C and 17°C in the winter and summer days, respectively. The warmer attic temperature (cases of sealed attic) can be good during winter period as it reduces heating load, and a disadvantage during the summer period as it increases cooling load. The opposite is true for highly ventilated attic roof.

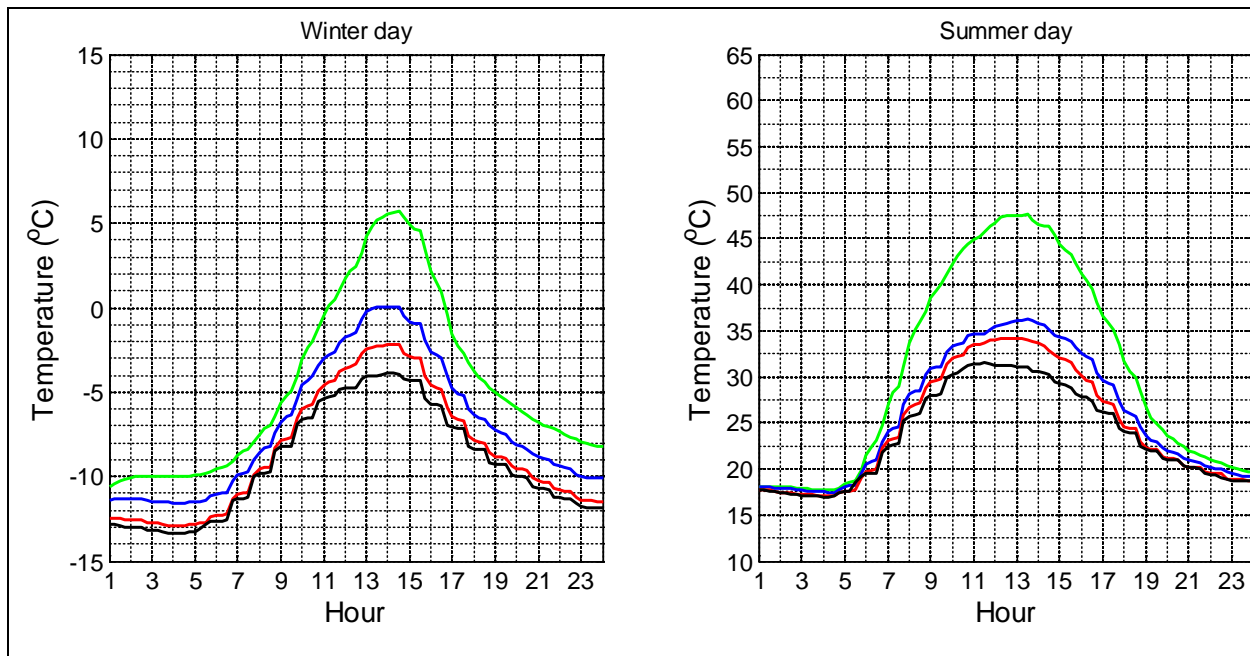


Figure 10 Average attic air temperature for different attic ventilation scenarios during a typical winter and summer day (Ottawa). Color code: green (sealed), blue (stack effect), red (0.6Pa wind pressure), black (2Pa wind pressure)

The maximum temperature of the roof sheathing during the winter and summer days considered in this study are shown in Figure 11. As can be seen in the figures, there is no significant difference in the roof temperatures of the four cases. The daily temperature fluctuations during the winter and the summer days are about 23°C and 43°C, respectively. These high daily temperature fluctuations can have an impact on the service life of the roof shingles.

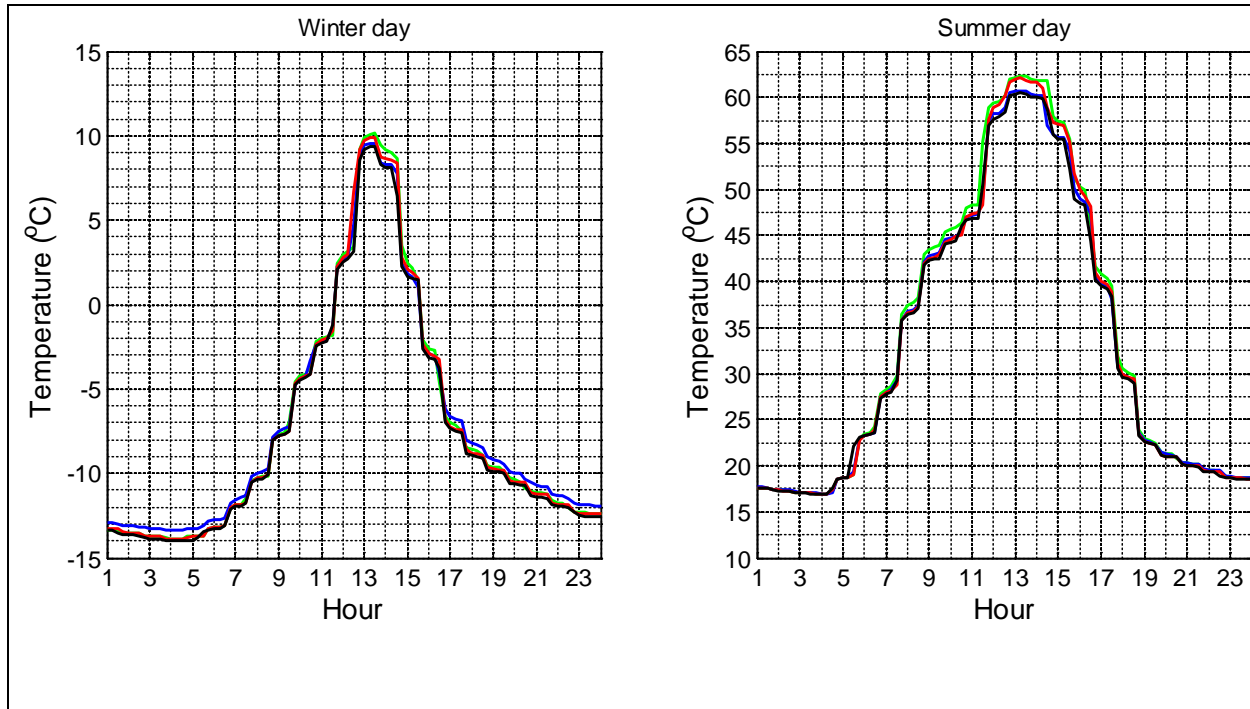


Figure 11 Maximum roof sheathing for different attic ventilation scenarios during a typical winter and summer day (Ottawa). Color code: green (sealed), blue (stack effect), red (0.6Pa wind pressure), black (2Pa wind pressure)

6.3 Attic Ventilation Rates

The amount of attic ventilation, in air-exchange per hour (ACH), which is expected in a typical winter and summer day under different wind conditions, are presented in Figure 12. In the absence of wind and solar gain, buoyancy induced ventilation yields about 4 ACH during the winter and 1.5 ACH in the summer day. As shown in Figure 13, attic air change per hour increases as solar radiation increases. For the same solar gain, the ACH in the winter is higher than summer, which must be attributed to the enhanced buoyancy flow due to higher temperature differences in the winter. For the boundary conditions considered in this report, the total air change per day in the winter is about 10% higher than the summer day, and in both cases the highest ventilation rates are under 7 ACH. In the cases where the attic is exposed to 0.6 Pa and 2 Pa wind pressure, the ventilation rate in the winter increases by 2.5 and 5.0 times of the case with no wind pressure (only stack effect), Figure 12. The wind induced ventilation rates during the winter and summer days are nearly the same: 9 - 10 ACH and 19 - 20.5 ACH for the case of 0.6 Pa and 2 Pa wind pressure, respectively. The nearly constant ventilation rate shown in Figure 12 suggests that, unlike the stack only ventilation case, the wind induced ventilation is less sensitive to solar gain.

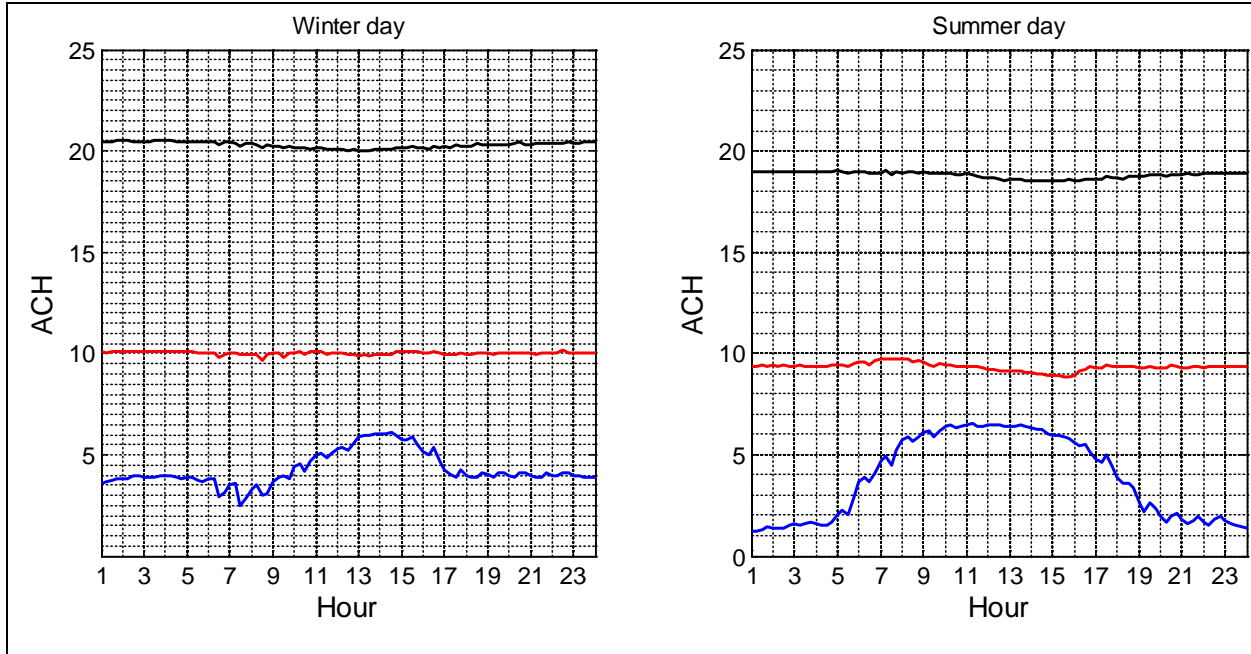


Figure 12 Attic ventilation rates for different attic ventilation scenarios during a typical winter and summer day (Ottawa). Color code: blue (stack effect), red (0.6Pa wind pressure), black (2Pa wind pressure)

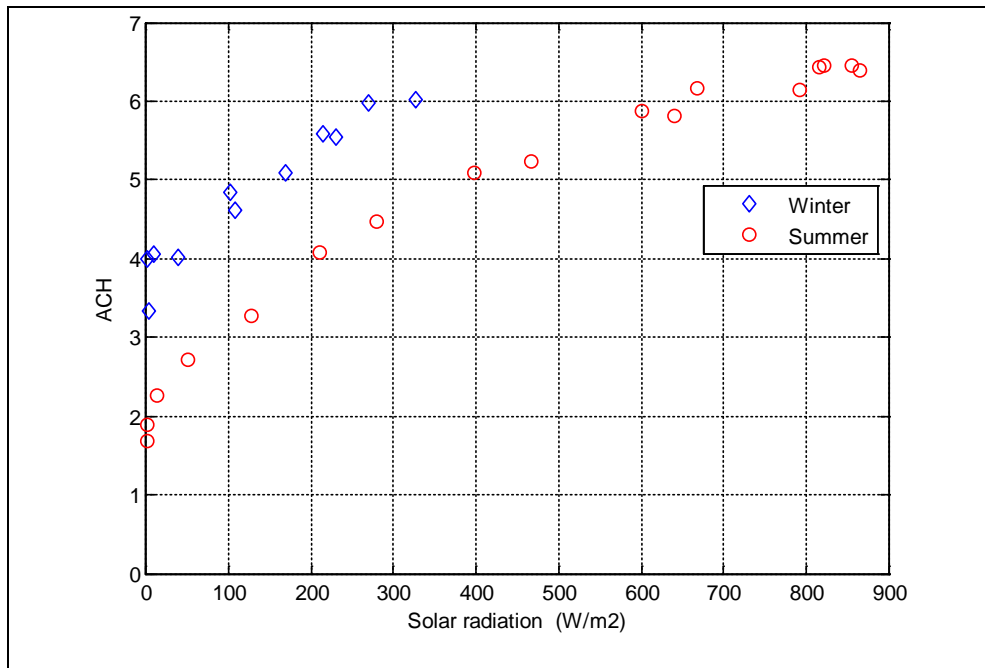


Figure 13 Effect of solar radiation in attic ventilation rate (for cases with stack effect)

6.3.1 Effect of Insulation Thickness on Attic Ventilation

To investigate the effect of attic insulation thickness on attic ventilation rate, two additional simulation cases with R45 (RSI-7.9) and R60 (RSI- 10.6) were carried out. Figure 14 shows the massflow rates and the ACH at different hours in the attic roof with R30, R45 and R60. The figure on the left (Figure 14) shows as insulation thickness increases, the airflow rate through the attic space tends to slightly decrease. This must be attributed due to the reduction in heat flow from the conditioned space to the attic space, which results low insulation surface and attic air temperatures. Although the flow rate slightly decreases with insulation thickness, as can be seen in the figure on the right (Figure 14), the ACH is slightly higher in the attic with higher insulation values when solar radiation gain is higher. The main reason for the slight increase in ACH is due to reduction in attic space volume due to the addition of extra insulation thickness. In general, however, the attic ventilation rates in the three simulation cases are not significantly different.

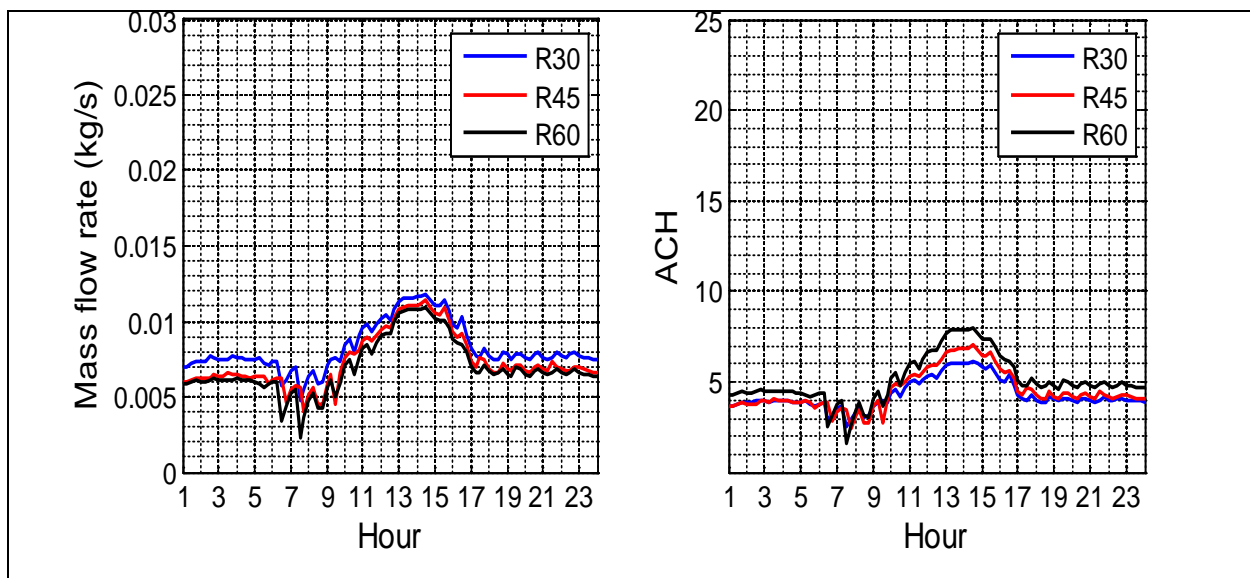


Figure 14 Attic ventilation rates with different insulation thickness

6.3.2 Effects of Baffle Size in Attic Ventilation

Most building codes recommend, as long as the insulation is not blocking the free air flow passage, a minimum of 1 inch gap between the roof sheathing and the insulation is considered sufficient. To investigate the effect of baffle size (air gap) on attic ventilation, in this project, three simulation cases with 1” (25 mm), 2” (50 mm) and 3” (75 mm) baffle were considered. The simulation results suggest that varying the baffle size influences the attic air distribution but has a lesser effect on

attic air temperature. Figure 16 shows the air distribution of three different baffle sized attics during a summer condition and wind speed of 2 m/s entering through the left soffit vent. As shown in the figure, the air velocity in the attic increases as the baffle size increases. The flow patterns in the corresponding attics are also quite different. The air change per hour values of the three cases are presented in Figure 15. From the graph it can be deduced that the gap between the underside roof sheathing and insulation has significant influence in attic air change when the ventilation is driven by wind. The ACH value increases as the baffle size increases. The ACH in the attic with 2” and 3” baffle sizes are found to be 38.5% and 52.5%, respectively, higher than that of an attic with 1” baffle size. Similar simulation results suggest that the effect of baffle size is not significant when the ventilation is driven by stack-effect. In buoyancy driven ventilation case, the airflow is caused by the difference of the top of insulation and roof sheathing temperatures. This makes the change in baffle size to not considerably affect the air flow distribution and ACH.

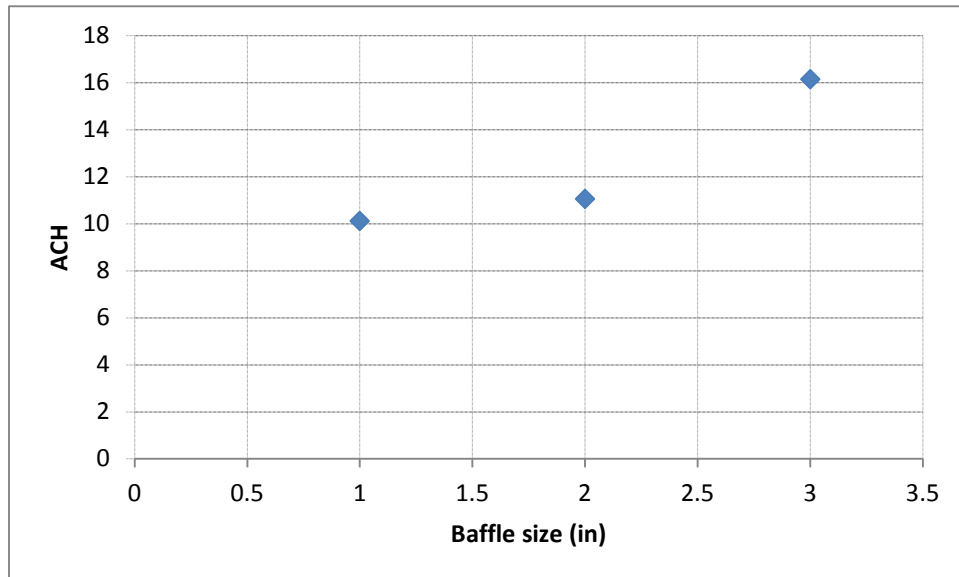


Figure 15 Attic ventilation (ACH) vs attic baffle size

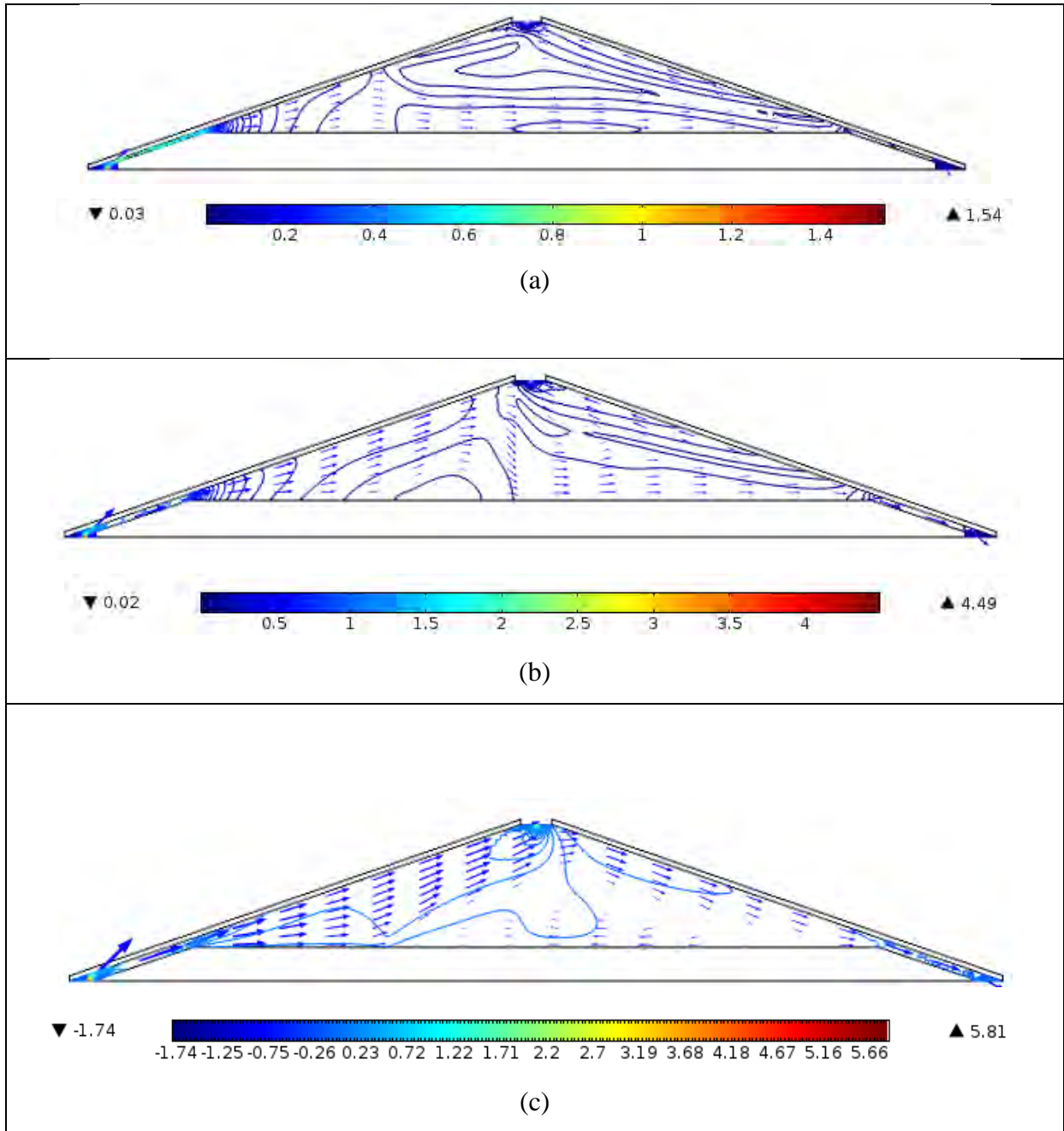


Figure 16 (a) - (c) air distribution in wind driven attic ventilation with an attic of baffle size 1 in, 2 in and 3 in respectively

6.4 Heat Flow through Attic Floor

Figure 17 shows the heat fluxes along the attic floor length at 12:00 am for the sealed attic, buoyancy and wind induced attic ventilation cases. The sharp increase in heat flux close to the ends is due to the two-dimensional heat flow and the reduced insulation thickness at the edges. The heat flux profiles away from the edge seem to correlate with the airflow patterns shown at the same time, Figure 8. Although not that significant, the locations where two airflow patterns meet in the sealed and buoyancy driven attic ventilation cases (Figure 8, a and b), are the same locations where slight changes in the heat flux profiles are observed in Figure 17. Similarly, the points where the cold air jet touch down the insulation in the cases of wind induced attic ventilation cases (Figure 8, c and d), are the same points where the heat fluxes show increase in the corresponding cases.

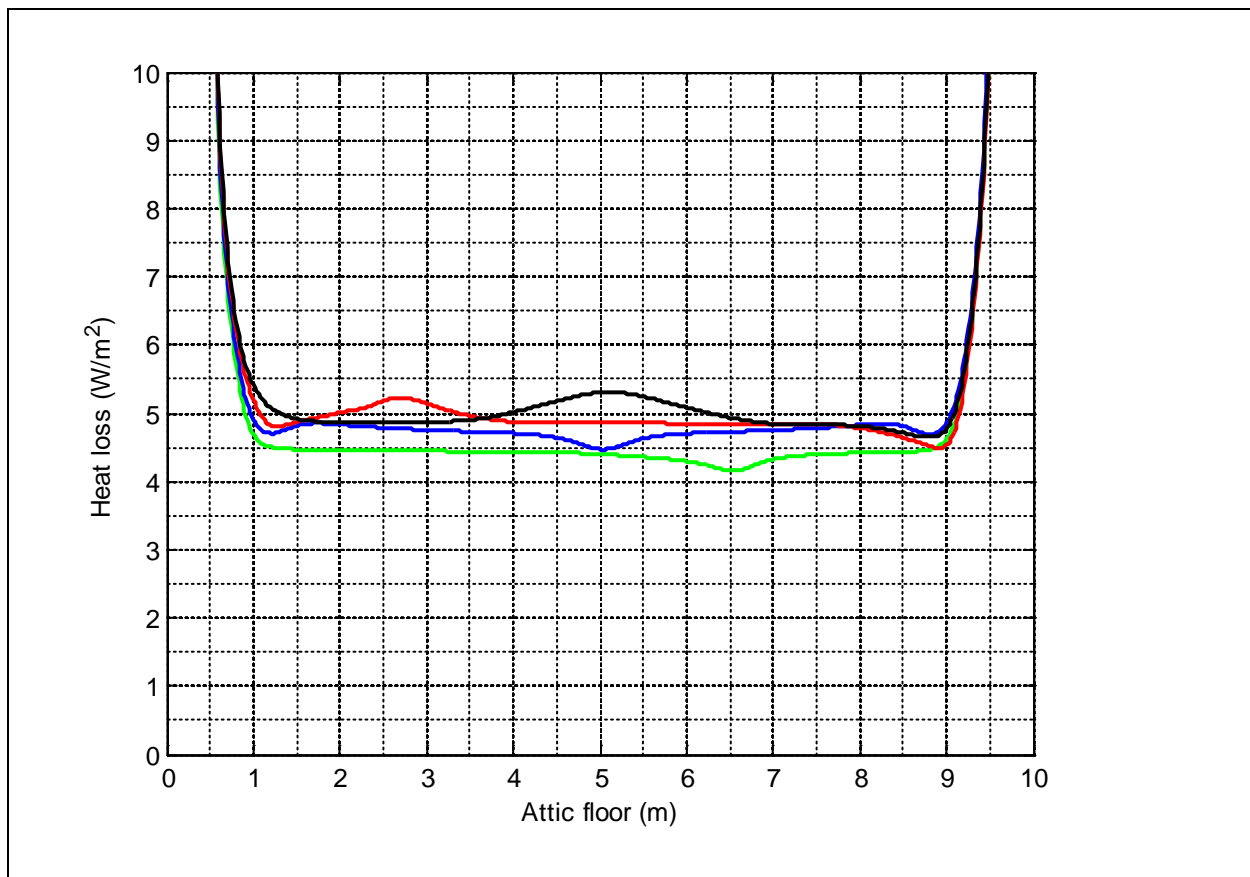


Figure 17 Heat flux along the attic floor at 12:00 am (winter day--Ottawa). Color code: green (sealed), blue (stack effect), red (0.6Pa wind pressure), black (2Pa wind pressure)

The hourly heat loss and gain through the attic roof during the winter and summer days, respectively, are presented in Figure 18. As can be seen in both figures, heat flow through sealed attic is higher than in both the buoyancy and the wind ventilated attic roofs. The heat flux difference among the four cases reaches the highest at 4:00 pm. This time corresponds to the lowest and the highest heating and cooling demands in the winter and summer days, respectively. The thermal energy storage capacity of sealed attic is beneficiary in the winter while it is disadvantageous in the summer period as it increases cooling load. Based on the boundary conditions used in this report, the daily total heat loss through the attic floor in winter in cases with buoyancy driven, 0.6 Pa and 2 Pa wind pressure conditions are 6.8%, 9.6% and 11.6%, respectively, higher than that of the sealed attic. In the summer, the cooling loads in the corresponding vented attic operation conditions decreases by 39%, 40% and 46%, respectively, when compared to sealed attic. As can be seen in the figures, higher attic ventilation rates due to wind pressure 10 ACH (0.6 Pa pressure) and 20 ACH (2 Pa wind pressure) does not significantly change the heating and cooling demands. In fact, from the energy saving (both heating and cooling) perspective, attic roof with only buoyancy driven ventilation (sheltered from wind) may perform better. Of course, for attic moisture control higher attic ventilation rates may be preferred.

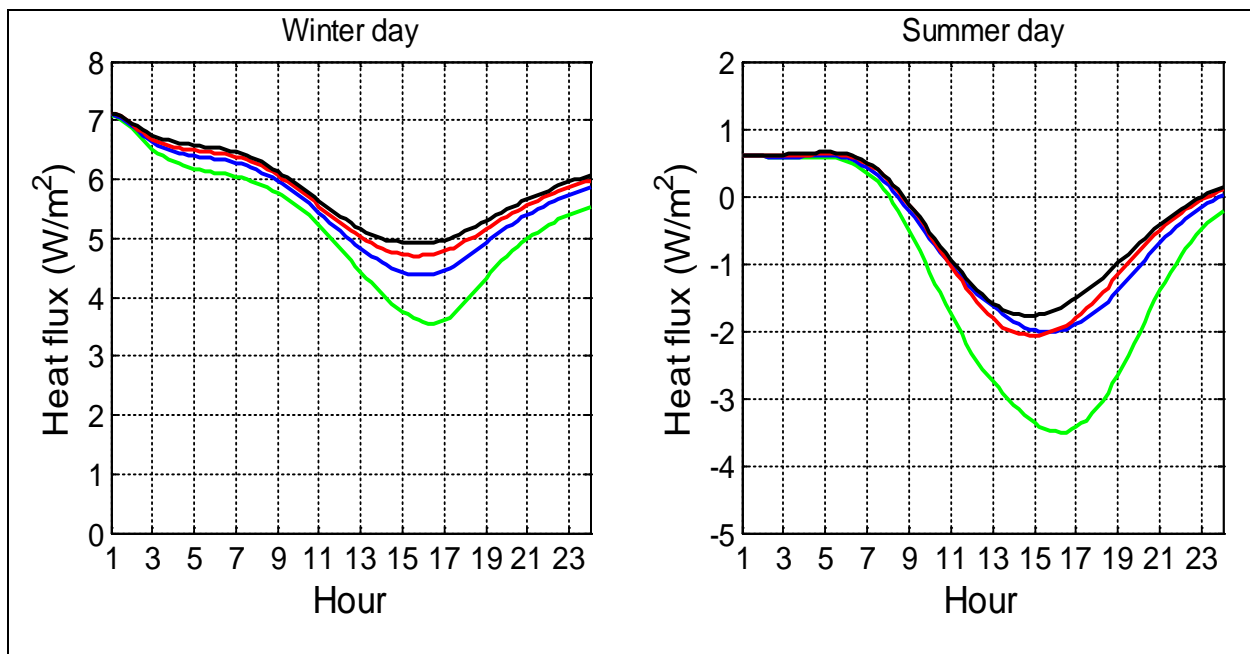


Figure 18 Hourly heat flux through attic floor for different attic ventilation scenarios during a typical winter and summer day (Ottawa). Color code: green (sealed), blue (stack effect), red (0.6Pa wind pressure), black (2Pa wind pressure)

7 Conclusion

In this report, the behaviors of air circulation and temperature profile inside attic and on attic structural elements are examined. A two-Dimensional CFD model using COMSOL is developed and benchmarked against existing experimental data. The air exchange per hour (ACH) in attic space under four different ventilation pressure cases are computed. In the absence of wind and solar gain, buoyancy induced ventilation in the winter is more than two times of that of the summer. In the absence of wind, attic ventilation increases as solar radiation increase. For wind pressure of 0.6 Pa and 2 Pa, the attic ventilation rate in the winter increases by 2.5 and 5.0 times of the case with no wind pressure (only stack effect). Unlike the buoyancy induced ventilation case, the wind induced ventilation is less sensitive to solar gain. In general, baffle size (size of air gap between roof sheathing and insulation) have impact on attic ventilation rate and airflow distribution but has a lesser effect on attic air temperature. The effect of baffle size is not significant when the ventilation is driven by stack-effect. The airflow path and temperature field in attic space are significantly affected by solar gain. In the absence of solar gain, relative high wind pressure (2 Pa in this report) forces the incoming air to flow underneath of the sheathing and exit at the ridge vent, which consequently reduces the time of residence of the incoming air and its subsequent mixing with the air in the attic space. The simulation results also show that attic ventilation in winter poses an energy penalty, whereas as in the summer it helps to remove the hot air from the attic space and reduce cooling load and energy demand.

8 References

1. L. V. Teesdale, *Condensation in Walls and Attics*, American Builder & Building Age, 1937.
2. T.S., Rogers, *Preventing Condensation in Insulated Structures*, Architectural Record, March 1938, pp. 109-119.
3. D. L. Roodvoets, *Practical Implications of the Elimination of Natural Attic Ventilation in Mixed Climates*, Performance of Exterior Envelopes of Whole Buildings VIII Conference Proceedings (ASHRAE), Florida, December 2001.
4. T.W. Forest and I. S. Walker, *Attic Ventilation and Moisture*, Final Report submitted to Canada Mortgage and Housing Corporation, 1993.
5. P. Roppel, N. Norris, M. Lawton, *Highly Insulated, Ventilated, Wood-Framed Attics in Cool Marine Climates*, Thermal Performance of the Exterior Envelopes of Whole Buildings XII International Conference, December 1-5, 2013, Clearwater Beach, Florida
6. J. Lstiburek, *Understanding Attic Ventilation*,
<http://www.buildingscience.com/documents/digests/bsd-102-understanding-attic-ventilation>,
retrieved, October 2014.
7. B. A Peavy, *A Model for Predicting the Thermal Performance of Ventilated Attics*, in *Summer Attic and Whole-House Ventilation*, NBS Special Publication 548, (1979), pp. 119–149
8. K. E. Wilkes, *Modeling of Residential Attics*, Thermal Performance of the Exterior Envelopes of Buildings, ASHRAE SP 28, American Society of Heating, Refrigerating, and Air-Conditioning Engineers, Inc., (1979), pp. 436–455.
9. K. E. Wilkes, *Dynamic Thermal Performance of Walls and Ceilings/ Attics*, Proceedings, ASHRAE/DOE Conference on Thermal Performance of the Exterior Envelopes of Buildings II, ASHRAE SP 38, (1983), pp.131–159.
10. ASTM Standard Practice C1340/C1340M – 10, *Estimation of Heat Gain or Loss through Ceilings under Attics Containing Radiant Barriers by Use of a Computer Program*, Current edition approved June 1, 2010.
11. S. Wang, Z. Shen, *Impacts of Ventilation Ratio and Vent Balance on Cooling Load and Air Flow of Naturally Ventilated Attics*. Energies 2012, 5, pp 3218-3232.

12. S. Wang, Z. Shen and L. Gu, *Numerical Simulation of Buoyancy-Driven Turbulent Ventilation in Attic Space under Winter Conditions*, *Energy and Buildings*, (2012), 47, pp 360-368.
13. A. Gagliano, F. Patania, A. Ferlito, F. Nocera, A. Galesi, *Computational Fluid Dynamic Simulations of Natural Convection in Ventilated Facades*, (2011) Chapter In book: *Evaporation, Condensation and Heat transfer*.
14. G.S. Gutt, *Condensation in Attics: Are Vapor Barriers Really the Answer*, *Energy and Buildings*, 1979, 2 (4), 251-258.
15. L. Susantia, H. Hommab, H. Matsumoto, *A Naturally Ventilated Cavity. Roof as Potential Benefits for Improving Thermal Environment and Cooling. Load of a Factory Building*, *Energy and Buildings*, 2011, 43, pp 211-218.
16. W. Tobiasson, J. Buska, A. Greatorex, *Ventilating Attics to Minimize Icings at Eaves*, *Energy and Buildings*, 1994, 21 (3), 360-368.
17. Q. Chen, *Prediction of Room Air Motion by Reynolds-Stress Models*, *Building and Environment*, 31, 233-244, 1996
18. R. D. Flack, C. L. Witt, *Velocity Measurements in Two Natural Convection Air Flows using a Laser Velocimetry*. *ASME J. Heat Transf.* 1979, 101, 256–260.
19. R. D. Flack, *The Experimental Measurement of Natural Convection Heat Transfer in Triangular Enclosures Heated or Cooled from Below*, *ASME J. Heat Transf.* 1980, 102, 770-772
20. BC Building and Plumbing Code – 2012, www.bccodes.ca/ retrieved September, 2, 2014.
21. ASHRAE Handbook Fundamentals, American Society of Heating and Air-Conditioning Engineers, Atlanta, 2013
22. N. Khan, Y. Su, S. B. Riffat, *A Review on Wind Driven Ventilation Techniques*, 2008, 40 (8), 1586-1604.

9 Appendix A: Simulation results for mild climate conditions

Attic temperature

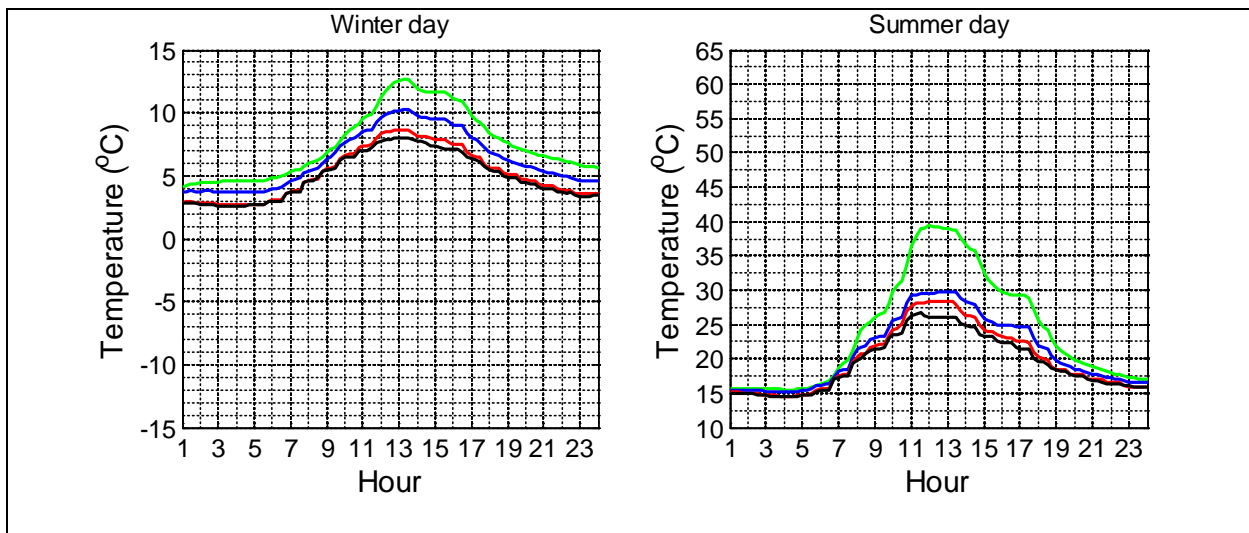


Figure 19 Average attic air temperature for different attic ventilation scenarios during a typical winter and summer day—Mild climate (Vancouver). Color code: green (sealed), blue (stack effect), red (0.6Pa wind pressure), black (2Pa wind pressure)

Roof sheathing temperature

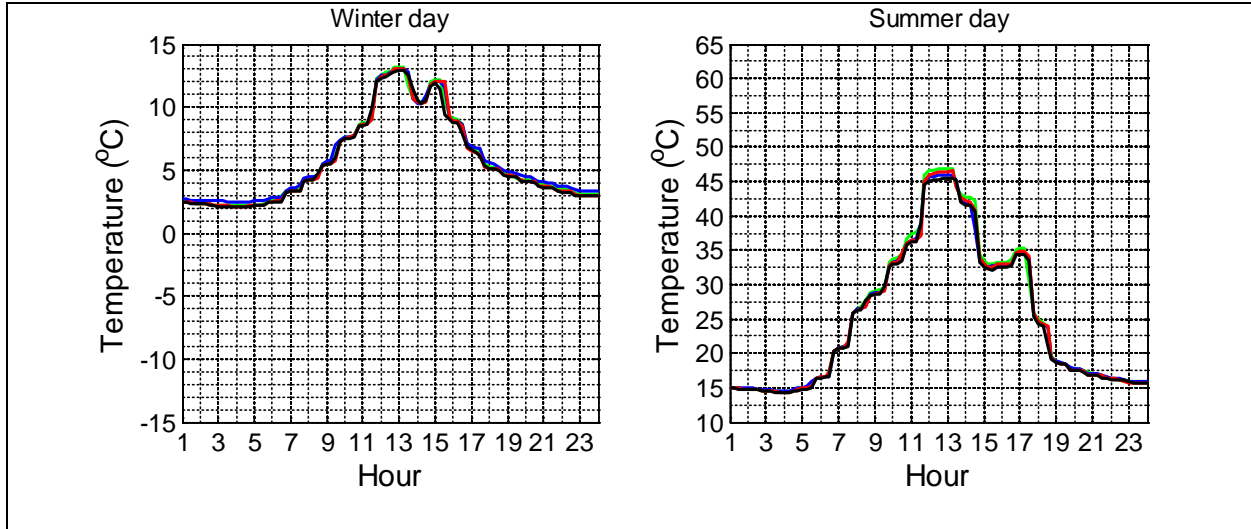


Figure 20. Maximum roof sheathing temperature for different attic ventilation scenarios during a typical winter and summer day—Mild climate (Vancouver). Color code: green (sealed), blue (stack effect), red (0.6Pa wind pressure), black (2Pa wind pressure)

Attic ventilation rate

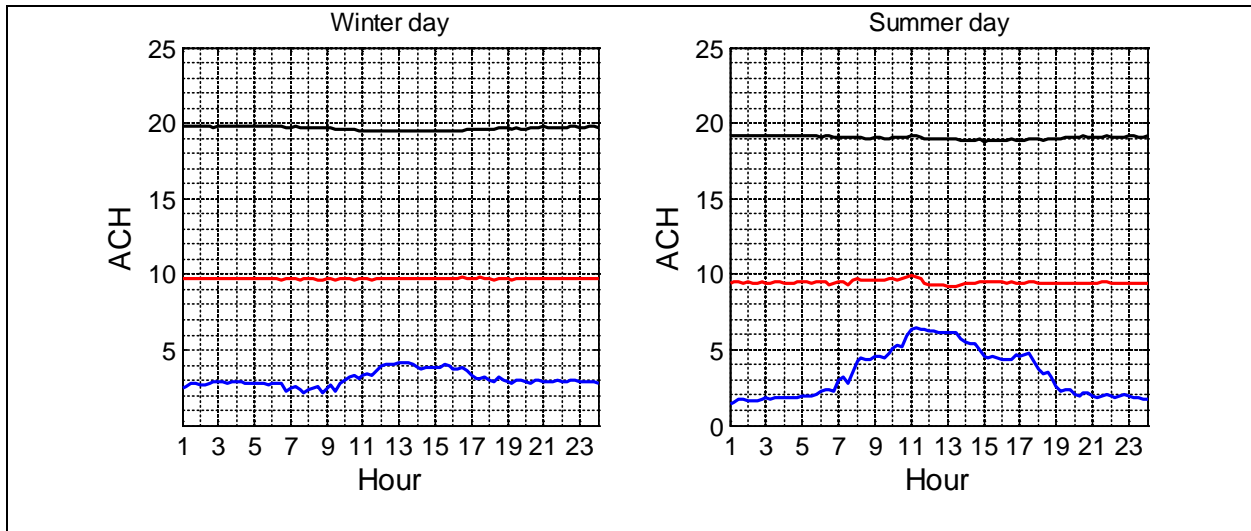


Figure 21 Attic ventilation rates for different attic ventilation scenarios during a typical winter and summer day—Mild climate (Vancouver). Color code: blue (stack effect), red (0.6Pa wind pressure), black (2Pa wind pressure)

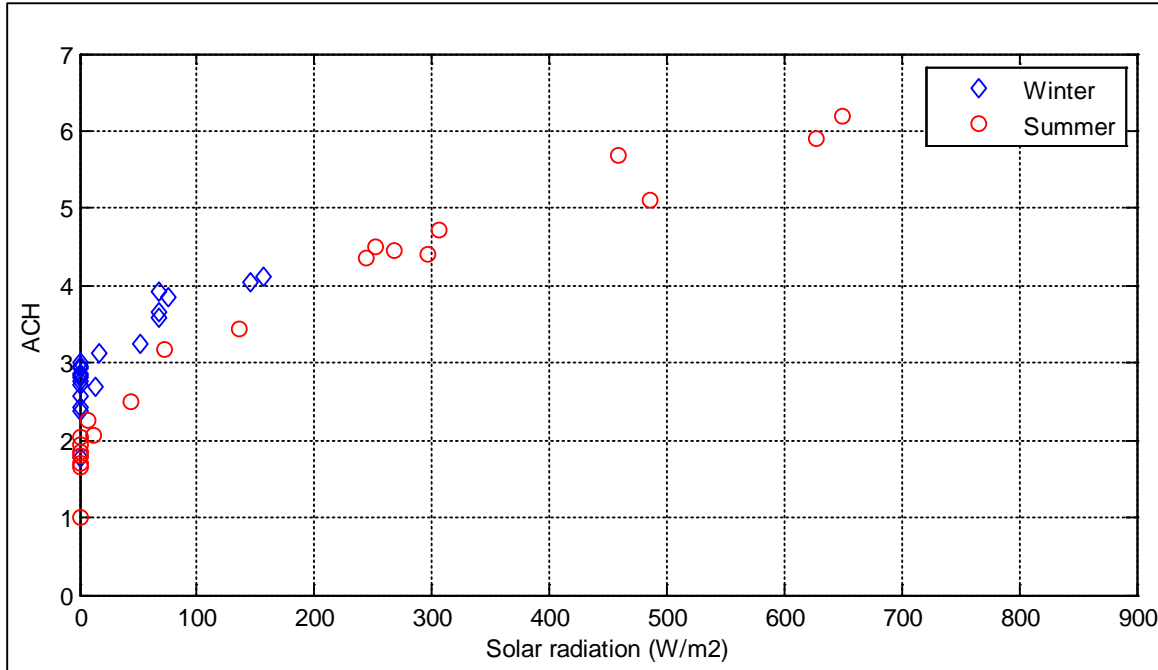


Figure 22 Effect of solar radiation in attic ventilation rate (for cases with stack effect)—Mild climate
Heat flow through attic floor

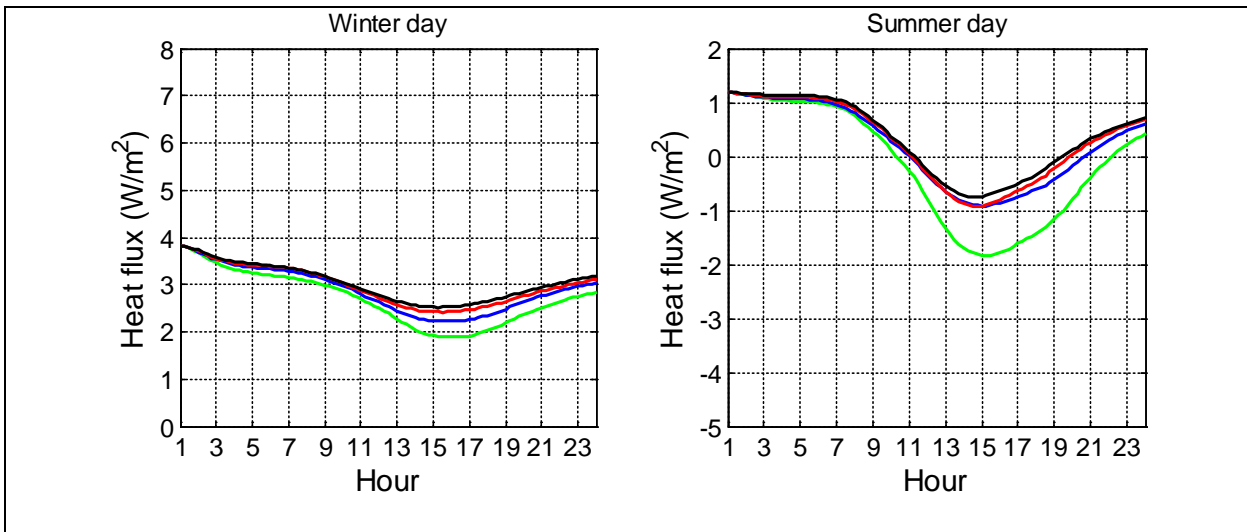


Figure 23 Hourly heat flux through attic floor for different attic ventilation scenarios during a typical winter and summer day—Mild climate (Vancouver). Color code: green (sealed), blue (stack effect), red (0.6Pa wind pressure), black (2Pa wind pressure)